6 Geothermometry and Geobarometry

The intersecting curves of the two classes (univariant curves for equilibria involving solids only and for equilibria involving a gas phase) will thus cut the general P–T diagram into a grid which we may call a petrogenetic grid. With the necessary data determined by experiment we might be able to locate very closely on the grid both the temperature and the pressure of formation of those rocks and mineral deposits of any terrane that were formed at a definite stage of its history, provided always that a sufficient variety of composition of materials occurred in the terrane to permit adequate cross reference. The determinations necessary for the production of such a grid constitute a task of colossal magnitude, but the data will be gradually acquired, and we shall thus slowly proceed toward an adequate knowledge of the conditions of formation of rocks and mineral deposits.

Bowen (1940)

In the previous two chapters we learned how to evaluate the thermodynamic properties of phases of fixed or variable compositions, and calculate changes in the thermodynamic properties of such phases involved in a chemical reaction. In this chapter we will learn how this knowledge may be applied for the estimation of temperature (*geothermometry*) and pressure (*geobarometry*) of equilibration of a given mineral assemblage at some point in its history, an application of prime interest to geologists. Such information provides quantitative constraints on *P–T* environments of geologic events such as magmatic crystallization, prograde and retrograde metamorphism, and formation of ore deposits. A mineral or mineral assemblage useful for geothermometry is called a *geothermometer*; one useful for geobarometry, a *geobarometer*. As most reactions are sensitive to both temperature and pressure, many authors refer to them as *geothermobarometers* or simply as *thermobarometers*.

6.1 Tools for geothermobarometry

Except for the use of fluid inclusions in minerals to obtain temperature (and, in some cases, pressure) information about the host minerals, the techniques employed for quantitative geothermometry and geobarometry rely on chemical reactions that have been calibrated as a function of temperature, or pressure, or both. A *petrogenetic grid*, as was conceived by Bowen (1940) several decades ago, is merely a collection of such calibrated reactions relevant to a portion of the *P–T* space. Petrogenetic grids are useful for estimating *P–T* limits of assemblages if the minerals are well approximated by reactions included in the grid.

The tools that have commonly been used for geothermobarometry are (Essene, 1982, 1989; Bohlen and Lindsley, 1987):

(1) univariant reactions, in which all phases essentially have fixed compositions, and *displaced equilibria*, in which one or more phases are solid solutions of variable compositions;
(2) exchange reactions, in which exchange of one element for another between two coexisting phases occurs primarily as a function of temperature;
(3) solvus equilibria, in which the solubility of a component in a phase varies as a function of temperature (or, less commonly as a function of pressure);
(4) study of cogenetic fluid inclusions in minerals;
(5) fractionation (or partitioning) of oxygen or sulfur isotopes between coexisting phases, which is a function of temperature only except at very high pressures (see Chapter 11).

Reactions used for thermobarometry generally involve minerals of high variance in natural compositions (e.g., garnet,

Introduction to Geochemistry: Principles and Applications, First Edition. Kula C. Misra.

Table 6.1 Some commonly used geothermometers and geobarometers.

	Mineral assemblage	Reaction/basis	Selected references
Intercrystalline exchange reactions			
Mg^{2+}–Fe^{2+} exchange	Garnet–clinopyroxene	$1/3Mg_3Al_2Si_3O_{12}$ (py) + $CaFeSi_2O_6$ (hd) = $1/3\ Fe_3Al_2Si_3O_{12}$ (alm) + $CaMgSi_2O_6$ (diop)	Råheim and Green (1974); Ellis and Green (1979); Dahl (1980); Hodges and Spear (1982); Krogh (1988); Pattison and Newton (1989); Kitano *et al.* (1994); Berman *et al.* (1995); Ganguly *et al.* (1996); Holdaway *et al.* (1997); Holdaway (2000)
	Garnet–orthopyroxene	$Mg_3Al_2Si_3O_3$ (py) + $3FeSiO_3$ (fs) = $Fe_3Al_2Si_3O_3$ (alm) + $3MgSiO_3$ (en)	Mori and Green (1978); Harley (1984); Sen and Bhattacharya (1984); Aranovich and Berman (1997)
	Garnet–biotite (GABI)	$KMg_3Si_3AlO_{10}(OH)_2$ (phl) + $Fe_3Al_2Si_3O_{12}$ (alm) = $KFe_3Si_3AlO_{10}(OH)_2$ (ann) + $Mg_3Al_2Si_3O_{12}$ (py)	Ferry and Spear (1978); Perchuk and Lavrent'eva (1983); Hodges and Spear (1982); Indares and Martignole (1985); Berman (1990); Dasgupta *et al.* (1991); Bhattacharya *et al.* (1992); Kleeman and Reinhardt (1994); Berman and Aranovich (1996); Ganguly *et al.* (1996); Gessmann *et al.* (1997); Mukhopadhyay *et al.* (1997); Holdaway (2000)
	Garnet–olivine	$1/3Mg_3Al_2Si_3O_{12}$ (py) + $1/2Fe_2SiO_4$ (fa) = $1/3Fe_3Al_2Si_3O_{12}$ (alm) + $1/2Mg_2SiO_4$ (fo)	O'Neill and Wood (1979); Kawasaki and Matsui (1983); Hackler and Wood (1989); Ryan *et al.* (1996)
	Garnet–cordierite	$2Fe_3Al_2Si_3O_{12}$ (alm) + $3Mg_2Al_4Si_5O_{18}$ (Mg-cord) = $1/3Mg_3Al_2Si_3O_{12}$ (py) + $3Fe_2Al_4Si_5O_{18}$ (Fe-cord)	Currie (1971); Hensen and Green (1971); Thompson (1976); Holdaway and Lee (1977); Perchuk and Lavrent'eva (1983)
	Garnet–ilmenite	$Fe_3Al_2Si_3O_{12}$ (alm) + $3MnTiO_3$ = $Mn_3Al_2Si_3O_{12}$ (spess) + $3FeTiO_3$ (ilm)	Powneby *et al.* (1987); Anderson and Lindsley (1981)
	Olivine–orthopyroxene	$Mg_2Si_2O_6$ (en) + Fe_2SiO_4 (fa) = $Fe_2Si_2O_6$ (fs) + Mg_2SiO_4 (fo)	Von Seckendorff and O'Neill (1993)
	Olivine–clinopyroxene (calcic)	1/2 Mg_2SiO_4 (fo) + $CaFeSi_2O_6$ (hd) = $1/2Fe_2SiO_4$ (fa) + $CaMgSi_2O_6$ (diop)	Powell and Powell (1974); Perkins and Vielzeuf (1992); Kawasaki and Ito (1994); Loucks (1996)
	Olivine–spinel	$MgSi_{0.5}O_2$ (fo)+ $Fe(Y)O_4$ (sp) = $FeSi_{0.5}O_2$ (fa)+ $Mg(Y)O_4$ (sp) [Y = Al, Cr]	Engi (1983); Jameison and Roeder (1984); Sack and Ghiorso (1991)
	Orthopyroxene–biotite	$1/3KFe_3Si_3AlO_{10}(OH)_2$ (ann) + 1/2 $Mg_2Si_2O_6$ (en) = $1/3KMg_3Si_3AlO_{10}(OH)_2$ (phl) + 1/2 $Mg_2Si_2O_6$	Sengupta *et al.* (1990)
	Magnetite–ilmenite (FeO–TiO_2–O_2 system)	Fe_3O_4 (mt) + $FeTiO_3$ (ilm) = Fe_2TiO_4 (usp) + Fe_2O_3 (hem) $4Fe_3O_4$ (mt) + O_2 = $6Fe_2O_3$ (hem)	Buddington and Lindsley (1964); Spencer and Lindsley (1981); Bohlen and Lindsley (1987); Anderson and Lindsley (1988); Brown and Navrotsky (1994); Woodland and Wood (1994)
Mg^{2+}–NI^{2+} exchange	Olivine–orthopyroxene	$1/2Mg_2SiO_4$ (fo) + $NiSiO_3$ = $1/2Ni_2SiO_4$ + $MgSiO_3$ (en)	Medaris (1968); Podvin (1988); von Seckendorff and O'Neill (1993); Ganguly and and Tazzoli (1994)
	Olivine–basaltic melt	$1/2Mg_2SiO_4$ (fo) + NiO (melt)= $1/2Ni_2SiO_4$ + MgO (melt)	Duke (1976); Hart and Davis (1978); Hirschman (1991); Roeder andEmslie (1970); Irvine (1975)
Univariant reactions and displaced equilibria			
	Andalusite–sillimanite–kyanite	andalusite = sillimanite; sillimanite = kyanite; kyanite = andalusite	Holdaway (1971); Hodges and Spear, 1982; Bohlen *et al.* (1991); Hemingway *et al.* (1991); Holdaway and Mukhopadhyay (1993) Harlov and Newton (1993); Whitney (2002)
	Orthopyroxene–olivine–quartz	$2FeSiO_3$ (fs) = Fe_2SiO_4 (fo) + SiO_2 (qz)	Bohlen *et al.* (1980a, 1980b); Davison and Lindsley (1989)

Clinopyroxene–plagioclase–quartz	$NaAlSi_3O_8$ (alb/analbite) = $NaAlSi_2O_6$ (jd) + SiO_2 (qz)	Ganguly (1973); Holland (1980); Newton (1983)
Garnet–orthopyroxene (Al content of opx in equilibrium with garnet)	$Mg_2Si_2O_6$ (en) + $MgAl_2Si_2O_6$ (Mg-Tschermak, MgTs) = $Mg_3Al_2Si_3O_{12}$ (py)	Wood and Banno (1973); MacGregor (1974); Harley (1984); Sen and Bhattacharya (1984); Lee and Ganguly (1988); Brey and Köhler (1990); Aranovich and Berman (1997); Taylor (1998)
Garnet–plagioclase–sillimanite /kyanite–quartz (GASP)	$3CaAl_2Si_2O_8$ (an) = $Ca_3Al_2Si_3O_{12}$ (gr) + $2Al_2SiO_5$ (sil/ky) + SiO_2 (qz)	Ghent (1976); Ghent *et al*. (1979); Newton and Haselton (1981); Hodges and Spear (1982); Ganguly and Saxena (1984); Koziol and Newton (1988); Koziol (1989); Spear (1993); Holdaway (2001)
Garnet–plagioclase–orthopyroxene–quartz (GAPES)	$CaAl_2Si_2O_8$ (an) + $Mg_2Si_2O_6$ (en) = $2/3Mg_3Al_2Si_3O_{12}$ (py) + $1/3Ca_3Al_2Si_3O_{12}$ (gr) + SiO_2 (qz)	Newton and Perkins (1982); Bohlen *et al*. (1983a); Perkins and Chipera (1985); Eckert *et al*. (1991)
Garnet–plagioclase–clinopyroxene–quartz (GADS)	$CaAl_2Si_2O_8$ (an) + $CaMgSi_2O_6$ (diop) = $2/3Ca_3Al_2Si_3O_{12}$ (gr) + $1/3Mg_3Al_2Si_3O_{12}$ (py) + SiO_2 (qz)	Newton and Perkins (1982); Perkins and Chipera (1985); Moecher *et al*. (1988); Eckert *et al*. (1991)
Garnet–rutile–Al_2SiO_5 polymorph–ilmenite–quartz (GRAIL)	$Fe_3Al_2Si_3O_{12}$ (alm) + $3TiO_2$ (rut) = $3FeTiO_3$ (ilm) + Al_2SiO_5 (sil) + $2SiO_2$ (qz)	Bohlen *et al* (1983b)
Garnet–rutile–ilmenite–plagioclase–quartz (GRIPS)	$CaFe_2Al_2Si_3O_{12}$ (gr_1alm_2) + $2\ TiO_2$ (rut) = $2FeTiO_3$ (ilm) + $CaAl_2Si_2O_8$ (an) + SiO_2 (qz)	Bohlen and Liotta (1986)
Garnet–plagioclase–amphibole–quartz	$6CaAl_2Si_2O_8$ (an) + $3NaAlSi_3O_8$ (ab) + $3Ca_2Mg_5Si_8O_{22}(OH)_2$ (trem) = $2Ca_3Al_2Si_3O_{12}$ (gr) + $3NaCa_2Mg_4Al_3Si_6O_{22}(OH)_2$ (par) + $Mg_3Al_2Si_3O_{12}$ (py) + 18 SiO_2 (qz)	Kohn and Spear (1989)
Garnet–plagioclase–muscovite–biotite	$Mg_3Al_2Si_3O_{12}$ (py) + $Ca_3Al_2Si_3O_{12}$ (and) + $KAl_3Si_3O_{10}(OH)_2$ (mus) = $3CaAl_2Si_2O_8$ (an) + $KMg_3AlSi_3O_{10}(OH)_2$ (bi)	Ghent and Stout (1981); Hodges and Spear (1982); Hodges and Crowley (1985); Hoisch (1991)
Solvus equilibria		
Alkali feldspar–albite (two-feldspar thermometry)	The distribution of K and Na between alkali feldspar and albite coexisting in equilibrium	Stormer (1975); Whitney and Stormer (1977); Green and Udansky (1986); Fuhrman and Lindsley (1988); Holland and Powell (1992)
Alkali feldspar–plagioclase (ternary feldspar)	Limits of miscibility gap in the ternary system (or–ab–an)	Whitney and Stormer (1977); Ghiorso (1984); Fuhrman and Lindsley (1988); Elkins and Grove (1990)
Calcite–dolomite	The distribution of Mg and Ca between calcite and dolomite coexisting in equilibrium	Harker and Tuttle (1955); Goldsmith and Newton (1969); Powell *et al*. (1984); Anovitz and Essene (1987)
Clinopyroxene–orthopyroxene	The distribution of Ca and Mg between clinopyroxene and orthopyroxene coexisting in equilibrium	Lindsley (1983); Gasparik (1984b); Bertrand and Mercier (1985); Davidson and Lindsley (1985); Wood (1987); Carlson and Lindsley (1988); Brey and Köhler (1990)

Mineral abbreviations: act = actinolite, ab = albite, alm = almandine, and = andalusite, an = anorthite, ann = annite, bi = biotite; cal = calcite, cord = cordierite diop = diopside, en = enstatite, fs = ferrosilite, gr = grossular, hc = hercynite, hd = hedenbergite, hem = hematite, ilm = ilmenite, jd = jadeite, ksp = K-feldspar, ky = kyanite, mt = magnetite, mus = muscovite, or = orthoclase, par= pargasite, phl = phlogopite, py = pyrope, qz = quartz, rut = rutile, sil = sillimanite, sp = spinel, trem = tremolite, usp = ulvospinel.

pyroxene, feldspar), so that the corresponding thermodynamic equations are sliding scale or continuous *P–T* indicators. Garnet, a common mineral in medium- and high-grade metamorphic rocks, is a particularly useful mineral for both geothermometry and geobarometry. The equilibrium constants for Fe–Mg exchange reactions between garnet and most other silicates (such as clinopyroxene, biotite, etc.) have large values because of the strong preference of Fe^{2+} (relative to Mg^{2+}) for the garnet structure. This, in turn, results in significantly temperature-dependent Fe–Mg distribution coefficients, a favorable condition for geothermometry. The usefulness of garnet in geobarometry arises from the fact that it is a dense mineral favored at high pressures. The downside of using garnet is the uncertainty associated with the activity models formulated for this mineral, which can incorporate a variety of elements such as Mn, Ti, and Cr.

As discussed in several excellent reviews (Ferry, 1980: Essene, 1982, 1989; Newton, 1983; Finnerty and Boyd, 1987; Bohlen and Lindsley, 1987; Spear, 1989; Smith, 1999), the list of promising thermobarometers is a long one. Essene (1989), for example, listed 60 equilibria that may be useful for thermobarometry, some more than others for a given metamorphic facies. A selection from the more commonly used thermobarometers is summarized in Table 6.1; we will discuss a few examples from this list to illustrate the principles involved. Many computer programs are available for calculations relevant to many thermobarometers included in the list; two widely used programs, both of which can be accessed online, are: THERMOBAROMETRY (version 2.1, May 1999) by Frank Spear and Mathew Kohn (http:ees2.geo.rpi.edu/MetaPetaRen/Software/GTB_Prog/), and THERMOCALC (updated 03–24–2011) by Tim Holland, Roger Powell, and Richard White (http://www.metamorph.geo.uni-mainz.de/thermocalc/).

6.2 Selection of reactions for thermobarometry

All thermobarometric studies based on mineral assemblages embody two inherent assumptions: (i) the mineral assemblage under consideration was in equilibrium at some former *P–T* condition, which we wish to determine; and (ii) the assemblage either has remained essentially unchanged since then or can be reconstructed from textural and other information preserved in the rock. It is not easy to verify either of these assumptions. There is no way to prove equilibrium; an assemblage is assumed to be in equilibrium if such an assumption is compatible with a lack of textural and chemical evidence indicative of disequilibrium. A commonly employed test of equilibrium is the concordance of *P* and *T* calculated from a number of independent reactions constructed from a multimineral assemblage, at least within the limits of uncertainties of the thermobarometers used. The assumption of no subsequent change may be tested by using a particular geothermometer or geobarometer for different samples of the same rock collected from an area of fairly uniform *P–T* regime as inferred from other lines of evidence. One can always calculate a pressure or a temperature from an appropriate geobarometer or geothermometer, but the numbers may or may not actually pertain to the geologic event being investigated. For example, calculations based on the compositions of only the outer rims of adjacent phases in a metamorphic assemblage, a common practice in thermobarometric applications, may yield satisfactory estimates of *P–T* conditions during cooling or uplift, but not of peak metamorphism.

For a given mineral assemblage it is generally possible to write a number of mass-balanced chemical reactions involving components of the phases (minerals) present in the assemblage. Of these only some may be suitable for thermobarometry in a particular case. The selection of reactions is based on the following considerations:

(1) An accurate thermodynamic database must be available for the end-member components included in the reaction. It is advisable to use self-consistent data sets to avoid introducing systematic errors, although a self-consistent data set is not necessarily an accurate one.

(2) The reaction must be well calibrated based either on empirical data or on data obtained from reversed experiments (from which standard enthalpies and entropies can be extracted). Empirical calibration is derived from the composition of minerals in natural assemblages for which the equilibrium pressure and temperature have been, or can be, estimated by some other thermobarometer(s) such as a metamorphic isograd (Ferry, 1980), an invariant point (Hodges and Spear, 1982), or other equilibria (Ghent and Stout, 1981; Hoisch, 1990). Empirical calibration is much simpler than its experimental counterpart, and the results may be more readily applicable to complex natural systems. Such a calibration, however, may be saddled with large uncertainties in the independent *P–T* estimate, and it may not apply to rocks with significantly different bulk compositions. Carefully conducted experiments can provide more accurate calibration, but experiments are almost always performed on simple systems composed of end-member components. Thermodynamic properties of phases are obtained either directly from the experiments involving the reaction being considered (e.g., Holdaway, 2000), or from a self-consistent thermodynamic database developed using statistical methods (such as multiple regression) or mathematical programming methods applied to all experimental data available for numerous related compositional systems (e.g., Berman, 1990; Holland and Powell, 1998).

(3) In natural assemblages we often have to deal with *displaced equilibria*, which refer to variations in temperature and pressure of a reaction that results from one or

more phases being solid solutions of variable composition. Displaced equilibria increase the P–T stability range of an assemblage and, therefore, are more useful than univariant reactions involving only pure components. However, the extension of experimental data to solid solution phases in natural assemblage(s) requires suitable solution models for determining activity–composition relations. Unfortunately, there is still no consensus regarding the correct solution model even for most anhydrous mineral groups (including those frequently used in thermobarometry, such as olivine, pyroxene, plagioclase, and garnet). The task is more difficult for hydrous silicates (e.g., amphiboles and micas), because mixing models for such minerals are based largely on unreversed experimental data or on simple ionic mixing models that are generally not supported by reversed experiments (Essene, 1989, p. 3). In many cases, the formulation of appropriate mixing models for solid solutions poses the most difficult challenge in thermobarometry.

(4) In general, reactions involving a fluid phase are not suitable for thermobarometry because of a lack of accurate information about the fluid composition and the ratio of fluid pressure (P_f) to total pressure (P_{total}).

A recurring issue in connection with the composition–activity relationship in Fe-bearing minerals is the recasting of the total Fe obtained with electron microprobe analysis into Fe^{2+} and Fe^{3+} using some established procedure (e.g., Deer *et al*., 1966; Stormer, 1983; Spear and Kimball, 1984; Droop, 1987; Spear, 1993). For some minerals, such as olivine and orthopyroxene, all the Fe may be treated as Fe^{2+} without introducing much error; for others, such as clinopyroxene and spinel, Fe^{2+} can be estimated by normalizing the analysis to cations and calculating the Fe^{2+}: Fe^{3+} that will satisfy the oxygen stoichiometry (see example in section 6.5.3). This procedure does not produce unique solutions for micas and amphiboles because of different possible substitutions, nor can it be applied to minerals with cation vacancies in their crystal structures. In such cases, Fe^{2+}–Fe^{3+} should be measured directly by wet-chemical analysis or by Mossbaüer spectroscopy. In some cases, all that may be feasible is to assume a Fe^{2+}: Fe^{3+} ratio based on experience and the published literature.

6.3 Dependence of equilibrium constant on temperature and pressure

The ultimate theoretical basis of most geothermometers and geobarometers is the temperature and pressure dependence of the equilibrium constant of a reaction (K_{eq}). This is because the compositional variations in minerals and coexisting fluids are already incorporated in the calculation of K_{eq} at a specified condition of temperature and pressure. The total variation of K_{eq} with respect to temperature and pressure can be represented by the total derivative of $\ln K_{eq}$:

$$\mathrm{d} \ln K_{eq} = \left(\frac{\partial \ln K_{eq}}{\partial T}\right)_P \mathrm{d}T + \left(\frac{\partial \ln K_{eq}}{\partial P}\right)_T \mathrm{d}P \tag{6.1}$$

From the relation $-RT \ln K_{eq} = \Delta G_r^{\,0} = \Delta H_r^0 - T\Delta S_r^0$ (equations 4.62 and 5.37),

$$\ln K_{eq} = \frac{-\Delta G_r^0}{RT} = \frac{-\Delta H_r^0}{RT} + \frac{\Delta S_r^0}{R} \tag{6.2}$$

where the superscript "0" refers to the chosen standard state. It follows from equation (6.2) that a plot of $\ln K_{eq}$ against $1/T$ (at constant pressure) will have a slope of $-\Delta H_r^0/R$ and an intercept of $\Delta S_r^0/R$ (Fig. 6.1a). The magnitudes of $\Delta H_r^0/R$ and $\Delta S_r^0/R$ will vary with temperature, unless they are assumed to be independent of temperature [i.e., $(\Delta C_p^0)_r = 0$], in which case the plot will be a straight line with a uniform slope (Fig. 6.1b). In the latter case, the enthalpy and entropy change of a reaction can be estimated if the value of K_{eq} for the reaction is known at several different temperatures (at constant pressure).

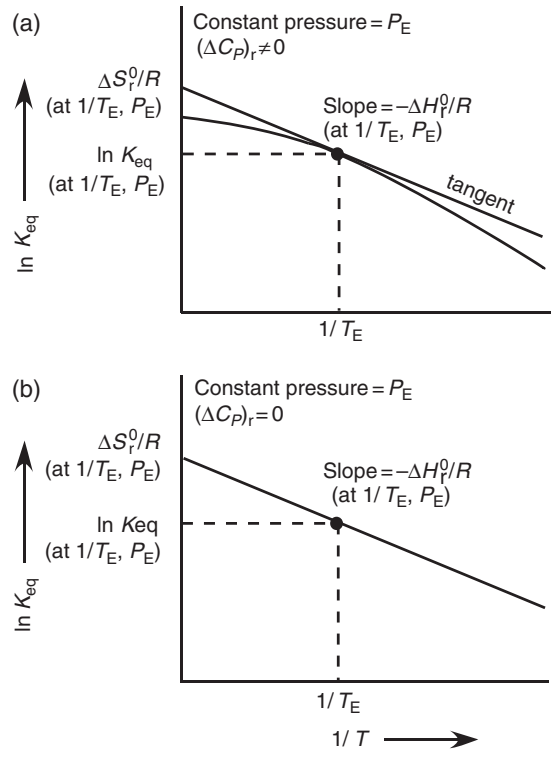

Fig. 6.1 Plot (schematic) of $\ln K_{eq}$ versus $1/T$ (K) at constant pressure with (a) $\Delta C_P \neq 0$ and (b) $\Delta C_P \neq 0$.

It can be shown (see Box 6.1) that the equation describing the dependence of K_{eq} on temperature at constant pressure, assuming ΔH_r^0 to be independent of temperature, is

$$\ln K_T = \ln K_{T\,\mathrm{ref}} - \frac{\Delta H_r^0}{R}\left(\frac{1}{T} - \frac{1}{T_{\mathrm{ref}}}\right) \tag{6.3}$$

The equation describing the dependence of K_{eq} on pressure at constant temperature, assuming ΔV_r^0 to be independent of temperature and pressure, is

$$\ln K_P = \ln K_{P\,\mathrm{ref}} - \frac{\Delta V_r^0}{RT}\left(P - P_{\mathrm{ref}}\right) \tag{6.4}$$

Box 6.1 Expressions for K_{eq} as a function of temperature and pressure (Krauskopf and Bird, 1995, pp. 203–210; Langmuir, 1997, pp. 20–23 and 28–30)

From equation (6.2), the variations of K_{eq} with temperature (at constant pressure) and with pressure (at constant temperature) are given by

$$\left(\frac{\partial \ln K_{eq}}{\partial T}\right)_P = -\frac{1}{R}\left(\frac{\partial\,(\Delta G_r^0 / T)}{\partial T}\right)_P = \frac{\Delta H_r^0}{RT^2} \quad \text{van't Hoff equation} \tag{6.5}$$

$$\left(\frac{\partial \ln K_{eq}}{\partial P}\right)_T = -\frac{1}{RT}\left(\frac{\partial\,\Delta G_r^0}{\partial P}\right)_T = -\frac{\Delta V_r^0}{RT} \tag{6.6}$$

The total change in K_{eq} with temperature at constant pressure is obtained by integrating equation (6.5) from some reference temperature (T_{ref}, usually taken as 298.15 K), for which ΔH_r and are known, to the temperature of interest, T:

$$\int_{T_{\mathrm{ref}}}^{T} \mathrm{d}(\ln K) = \ln K_T - \ln K_{T_{\mathrm{ref}}} = \int_{T_{\mathrm{ref}}}^{T} \frac{\Delta H_r^0}{RT^2}\,\mathrm{d}T \tag{6.7}$$

Assuming ΔH_r^0 to be independent of temperature [i.e., $(\Delta C_P^0)_r = 0$],

$$\ln K_T = \ln K_{T\,\mathrm{ref}} - \frac{\Delta H_r^0}{R}\left(\frac{1}{T} - \frac{1}{T_{\mathrm{ref}}}\right) \tag{6.3}$$

If this assumption is valid, a plot of $\ln K_T$ versus $1/T$ would yield a straight line with

$$\text{slope} = \frac{-\Delta H_r^0}{R} \qquad \text{and} \qquad \text{intercept} = -\ln K_{T_{\mathrm{ref}}} + \frac{\Delta H_r^0}{R}\,\frac{1}{T_{\mathrm{ref}}}$$

The linearity of such a plot would provide evidence that the assumption of constant ΔH_r^0 is justified. The value of ΔH_r^0 can then be evaluated from the slope of the plot. This method is used for obtaining enthalpy changes (at constant pressure) for reactions involving only condensed phases that would be difficult to measure directly.

If ΔH_r^0 varies with temperature, then its evaluation must take into account the variation of $(\Delta C_P^0)_r$ as a function of temperature, using analytical expressions, such as equation (4.53), for the C_P of each phase involved in the reaction. In the special case where $(\Delta C_P^0)_r$ = constant, , and the van't Hoff expression can be integrated to give

$$\ln K_T = \ln K_{T\,\mathrm{ref}} - \frac{\Delta H_r^0}{R}\left(\frac{1}{T} - \frac{1}{T_{\mathrm{ref}}}\right) - \frac{(\Delta C_P^0)_r}{R}\left[\left(\frac{T_{\mathrm{ref}}}{T} - 1\right) - \ln\frac{T_{\mathrm{ref}}}{T}\right] \tag{6.8}$$

The total change in K_{eq} with pressure at constant temperature is obtained by integrating equation (6.6) from some reference pressure (P_{ref}, usually taken as 1 bar), for which ΔV_r and are known, to the pressure of interest, P:

$$\int_{P_{\mathrm{ref}}}^{P} \mathrm{d}(\ln K) = \ln K_P - \ln K_{P_{\mathrm{ref}}} = -\int_{P_{\mathrm{ref}}}^{P} \frac{\Delta V_r^0}{RT}\,\mathrm{d}P \tag{6.9}$$

If, for simplicity, ΔV_r^0 can be assumed to be independent of temperature and pressure,

$$\ln K_P = \ln K_{P\,\mathrm{ref}} - \frac{\Delta V_r^0}{RT}\left(P - P_{\mathrm{ref}}\right) \tag{6.4}$$

In this case, a plot of $\ln Kp$ versus P would yield a straight line with slope $= -\Delta V_r^0/RT$ and intercept $= \ln K_{P\,\mathrm{ref}} + \frac{\Delta V_r^0}{RT} P_{\mathrm{ref}}$.

If ΔV_r^0 is a function of temperature and pressure, equation (6.4) has to be modified by taking into account the coefficient of thermal expansion at constant pressure (α_P) and the coefficient of compressibility at constant temperature (β_T) of the substances involved in the reaction (see Box 4.5).

For a reaction to qualify as a sensitive geothermometer, its equilibrium constant should be a function largely of temperature (i.e., almost independent of pressure); the opposite is the case for a potentially good geobarometer. It is evident from equation (6.5) that a sensitive geothermometer should have a large value of ΔH_r^0 (and a small value of ΔV_r^0). The larger the value of ΔH_r^0 (positive or negative), the more rapid is the change of K_{eq} with temperature. This means that an error in ΔH_r^0 or in the activity–composition relationships will produce a small error in the calculated T if ΔH_r^0 is large. Equation (6.6) indicates that a sensitive geobarometer, on the other hand, should have a large value of ΔV_r^0 (positive or negative). For rigorous thermobarometry it is advisable to consider heat-capacity data to calculate ΔH_r^0 and equation (4.74) or some other appropriate equation to calculate ΔV_r^0.

To determine the temperature or pressure from a univariant reaction, one of the two variables must be known from an independent source. For a given mineral assemblage, the intersection of two univariant reaction boundaries in P–T space, however, will fix both temperature and pressure, with the uncertainty of the estimates determined by the angle of intersection of the two reaction boundaries (Fig. 6.2).

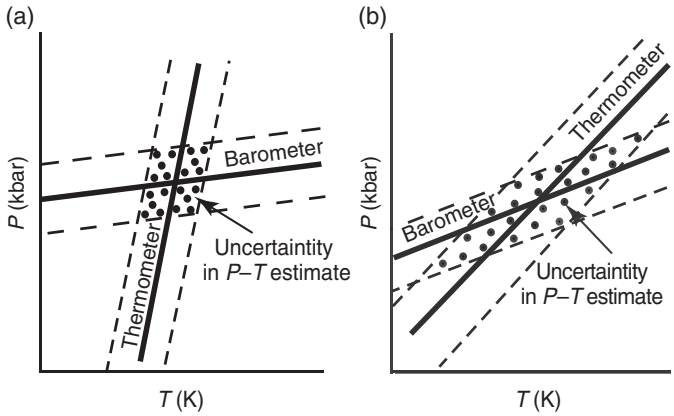

Fig. 6.2 Schematic illustration of thermobarometry from the intersection of two univariant reaction boundaries. The uncertainty in the position of each of the hypothetical reaction boundaries is shown by dashed lines and the uncertainties in the estimated pressure and temperature by the box with a pattern. Note that the uncertainties in the *P–T* estimate increase with a decrease in the angle of intersection, as in (a).

Example 6–1: Clinopyroxene–analbite equilibria as a function of pressure, temperature and the jadeite content of clinopyroxene

Consider the reaction that characterizes the equilibrium between omphacitic (Na-bearing) clinopyroxene (cpx) and disordered albite in blueschists, metamorphic rocks that are formed at high pressures and low temperatures in subduction zones. Representing the reaction in terms of end-member components,

$$\underset{\text{jadeite}}{\overset{\text{cpx}}{NaAlSi_2O_6}} + \overset{\text{quartz}}{SiO_2} \Leftrightarrow \overset{\text{analbite}}{NaAlSi_3O_8} \qquad (6.10)$$

the equilibrium constant for the reaction at pressure P and temperature T is given by

$$\Delta G^0_r = -RT \ln K_{eq} = -RT \ln \frac{a^{anb}_{NaAlSi_3O_8}}{a^{cpx}_{NaAlSi_2O_6}\, a^{qz}_{SiO_2}} \qquad (6.11)$$

In blueschists, jadeitic pyroxene exhibits a wide range of composition because of the components diopside ($CaMgSi_2O_6$) and acmite ($NaFe^{3+}Si_2O_6$) in solid solution. In contrast, quartz and analbite are nearly pure phases. Let us choose the standard state for each phase as the pure substance at P and T, so that $a^{qz}_{SiO_2} = 1$ and $a^{anb}_{NaAlSi_3O_8} = 1$. Let us also stipulate, as a first approximation, that the cpx solid solution is ideal and that the activity of jadeite can be approximated on the basis of a one-site mixing model: $a^{cpx}_{jd} = (X^{cpx}_{Na})^{M2}$ (Holland, 1979). Substituting the activity values in equation (6.11), we get

$$K_{eq} = 1/a^{cpx}_{NaAlSi_2O_6} = 1/X^{cpx}_{NaAlSi_2O_6} \qquad (6.12)$$

Thus, assuming that the pyroxene composition has not changed since its formation, the mole fraction of jadeite in the cpx solid solution will be a measure of the equilibrium constant at the pressure and temperature of metamorphism.

Assuming $(\Delta C_p)_r = 0$ and ΔV_r to be independent of temperature and pressure, ΔG_r at the chosen standard state (P, T) is given by (see equation 4.95)

$$\Delta G^0_r = \Delta G^P_{r,T} = \Delta H^1_{r,T} - T\,\Delta S^1_{r,T} + (P-1)\,\Delta V_r$$

so that the equation relating X^{cpx}_{jd}, P, and T (equation 6.12) can be written as

$$\ln K_{eq} = \ln \frac{1}{X^{cpx}_{jd}} = \frac{-\Delta G^0_r}{RT} = \frac{-\Delta H^1_{r,T}}{RT} + \frac{\Delta S^1_{r,T}}{R} - \frac{(P-1)\,\Delta V_r}{RT} \qquad (6.13)$$

We can use equation (6.13) to calculate P as a function of X^{cpx}_{jd} (or $\ln K_{eq}$) for any given temperature. For the purpose of illustration, the results for $T = 800$ K are presented in Table 6.2 and Fig. 6.3.

Similar calculations will yield a straight line in $P - \ln K_{eq}$ space for each chosen T, with the equilibration pressure being higher at higher temperatures for the same $X_{jd}{}^{cpx}$ (Fig. 6.3). Thus, if an independent estimate of temperature is available, the jadeite content of cpx in a clinopyroxene–albite–quartz assemblage can be used as a geobarometer (e.g., Reinsch,

Table 6.2 Thermodynamic data (Robie and Hemingway, 1995) and calculation of pressure for the clinopyroxene–analbite equilibria at T = 800 K as a function of clinopyroxene composition.

	Thermodynamic data			**Calculation of equilibrium *P* for the reaction**					
	$\Delta H^1_{f,T}$ **(kJ mol^{-1})**	S^1_T **(J mol^{-1} K^{-1})**	$V^1_{298.15}$ **(J bar^{-1})**	X^{cpx}_{jd}	**ln** K_{eq}	***P* (kbar)**	X^{cpx}_{jd}	**ln** K_{eq}	***P* (kbar)**
Jadeite	–3027.8	332.22	6.04	0.1	2.30	4.80	0.6	0.51	11.67
				0.2	1.61	7.46	0.7	0.36	12.26
Analbite	–3920.2	480.35	10.043	0.3	1.20	9.02	0.8	0.22	12.78
				0.4	0.92	10.12	0.9	0.11	13.23
Quartz	–907.4	99.83	2.269	0.5	0.69	10.97	1.0	0	13.63

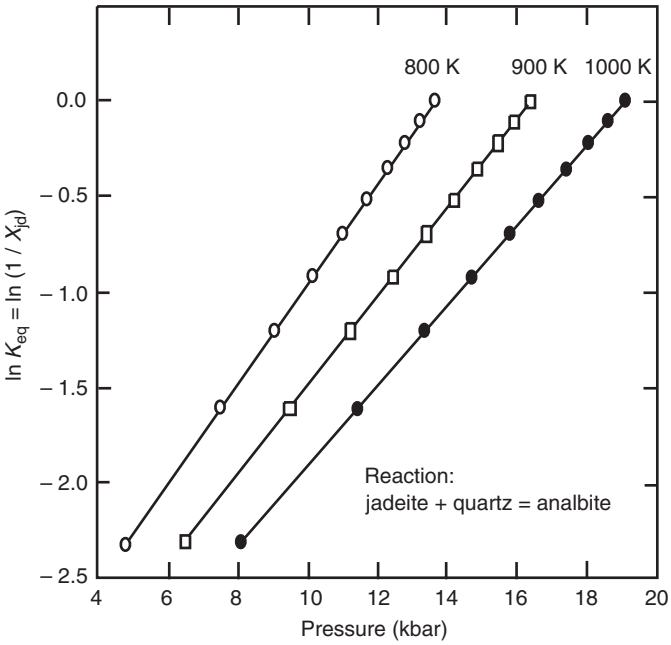

Fig. 6.3 Calculated relationship between ln K_{eq} and pressure for the reaction jadeite + quartz = analbite at constant temperatures 800 K, 900 K, and 1000 K. It is assumed that quartz and analbite are pure phases and clinopyroxene is an ideal solid solution with one mixing site.

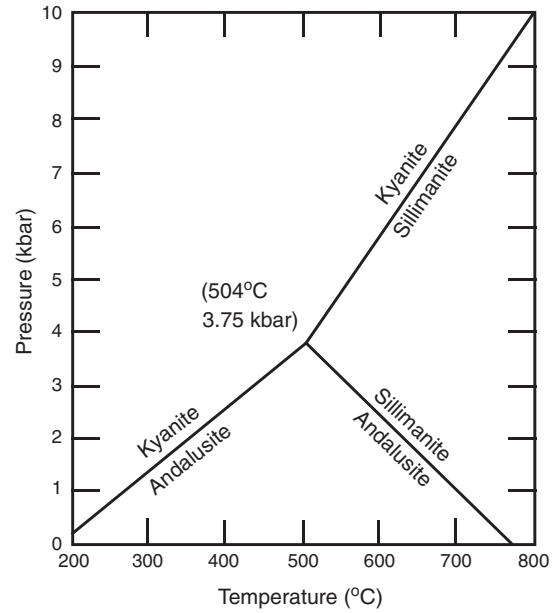

Fig. 6.4 The phase diagram for Al_2SiO_5 polymorphs (andalusite, kyanite, and sillimanite) as calculated by Holdaway and Mukhopadhyay (1993) from available thermodynamic data. The triple point is located at 504 ± 20°C and 3.75 ± 0.25 kbar. (After Holdaway and Mukhopadhyay, 1993, Fig. 5, p. 312.)

1977), provided the Na content of the cpx is measured accurately, for example, with an electron microprobe without any significant loss due to volatilization under the electron beam. The calculations, of course, will be a little more complicated for natural assemblages in which the plagioclase is not pure analbite or the cpx should not be assumed to behave as an ideal solid solution (see, e.g., Ganguly, 1973).

6.4 Univariant reactions and displaced equilibria

Univariant reactions and displaced equilibria involve consumption and production of phases and are referred to as *net transfer reactions*. The essence of thermobarometry based on such reactions is the determination of reaction boundaries as a function of temperature and pressure. The calculations, however, tend to get more cumbersome compared with the examples discussed above and in the previous two chapters. This is because most minerals in natural assemblages are solid solutions of variable composition, which generally do not conform to ideal mixing models.

6.4.1 Al_2SiO_5 polymorphs

One of the most commonly used thermobarometers for crustal rocks is based on the relative stabilities of the three Al_2SiO_5 polymorphs: andalusite, kyanite, and sillimanite. The phase diagram for this system consists of three univariant reaction boundaries (andalusite ⇔ sillimanite, sillimanite ⇔ kyanite, and kyanite ⇔ andalusite) that intersect at an invariant point (the triple point of the system) where all the three phases coexist in equilibrium at a specific set of *P–T* values. The phase relations in this system have been investigated experimentally by a number of workers (see reviews in Kerrick, 1990 (Chapter 3), and Holdaway and Mukhopadhyay, 1993); most petrologists now accept the reaction boundaries as determined by Holdaway and Mukhopadhyay (1993), who located the triple point at 504 ± 20°C and 3.75 ± 0.25 kbar (Fig. 6.4), not much different from some of the earlier determinations: 501 ± 20°C and 3.76 ± 0.3 kbar by Holdaway (1971); 503°C and 3.73 kbar by Berman (1988); and 511°C and 3.87 kbar by Hemingway *et al.* (1991).

Metamorphosed aluminous rocks, such as pelitic schists and micaceous quartzites, commonly contain one or more of these polymorphs. Assemblages containing only one of the polymorphs are not of much use in thermobarometry, but those containing any two of the three can be used as a geothermometer or a geobarometer, depending on whether the pressure or the temperature can be estimated from some other thermobarometer. Assemblages in which all three polymorphs coexist are not common, but have been reported (e.g., Grambling, 1981; Hiroi and Kobayashi, 1996; Whitney, 2002). In such a natural assemblage, the triple point of the Al_2SiO_5 phase diagram uniquely defines the equilibrium pressure and temperature, provided the Al_2SiO_5 phases are almost pure, and they formed contemporaneously.

A possible problem with the application of this thermobarometry is the Fe_2O_3 contents of andalusite and sillimanite, the effect of which is to increase the temperature of the andalusite ⇔ sillimanite reaction in proportion to the amount of Fe_2O_3 in the minerals undergoing reaction. Holdaway and Mukhopadhyay (1993) have cautioned that, with Fe_2O_3 as an impurity, the andalusite ⇔ sillimanite phase boundary may be up to 20°C higher than that in the pure aluminum silicate system. We should also remember that coexistence of the three polymorphs in a rock does not necessarily mean that they grew together at the *P–T* condition of the triple point. In some cases the textures clearly indicate a sequential growth of the polymorphs (Whitney, 2002).

6.4.2 *Garnet–rutile–Al_2SiO_5 polymorph–ilmenite–quartz (GRAIL) barometry*

A useful geobarometer is based on the natural assemblage garnet (gt)–rutile (rut)–Al_2SiO_5 polymorph (andalusite, kyanite, or sillimanite)–ilmenite (ilm)–quartz (qz) (commonly referred to as GRAIL) that is common in medium to high-grade, Al-rich metamorphic rocks. The equilibrium of interest in this case, with kyanite (ky) as the Al_2SiO_5 polymorph, can be written in terms of end-member components as

$$\underset{\text{almandine}}{\overset{\text{gt}}{Fe_3Al_2Si_3O_{12}}} + 3\overset{\text{rut}}{TiO_2} \Leftrightarrow 3\overset{\text{ilm}}{FeTiO_3} + \overset{\text{ky}}{Al_2SiO_5} + 2\overset{\text{qz}}{SiO_2} \qquad (6.14)$$

$$K_{eq} = \frac{\left(a^{\text{ilm}}_{FeTiO_3}\right)^3 \left(a^{\text{ky}}_{Al_2SiO_5}\right) \left(a^{\text{qz}}_{SiO_2}\right)^2}{\left(a^{\text{gt}}_{\text{alm}}\right) \left(a^{\text{rut}}_{TiO_2}\right)^3} \qquad (6.15)$$

The experimentally based *P–T* calibration of this reaction by Bohlen *et al.* (1983b) is shown in Fig. 6.5. The figure also shows contours of $\log_{10}K_{eq}$ calculated from the relation

$$\Delta P \cong -\frac{RT \log_{10} K_{eq}}{\Delta V_r} \qquad (6.16)$$

using available data on molar volumes, isobaric thermal expansion, and isothermal compressibility to calculate ΔV_r. Note that the slopes of the $\log_{10}K_{eq}$ contours change slightly when they pass from the stability field of one mineral to that of another. The very gentle d*P*/d*T* slopes of the $\log_{10}K_{eq}$ contours translate to a maximum error of only about 0.5 kbar in the inferred pressure corresponding to temperature uncertainties of ±50°C; this is the reason why the GRAIL equilibrium qualifies as a sensitive geobarometer. We can use the $\log_{10}K_{eq}$ contours in Fig. 6.5 to estimate the equilibration pressure of a given GRAIL assemblage, provided (i) the assemblage can be inferred to have coexisted in equilibrium, (ii) we can obtain a reasonable estimate of the equilibration temperature of the assemblage from some geothermometer (e.g., garnet–biotite exchange reaction), and (iii) we have appropriate solution models to calculate activities of the end-member components in impure minerals and thus K_{eq} for the assemblage. However, the $\log_{10}K_{eq}$ contours in Fig. 6.5, derived from experimental data, are not dependent on the mixing models for the solid solutions in the reaction, and potential users can make their own choice of solution models for geobarometry applications.

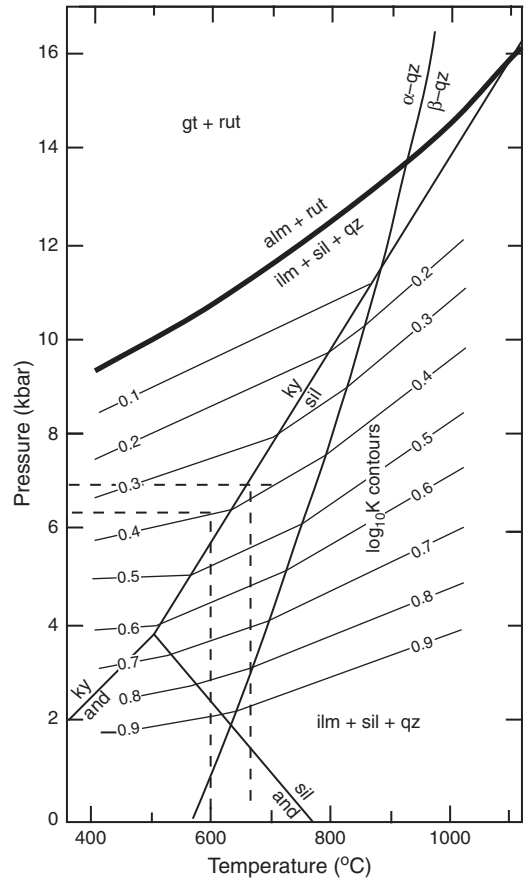

Fig. 6.5 Pressure–temperature diagram showing the experimentally based univariant reaction boundary for the GRAIL equilibrium (equation 6.9) involving only pure phases, and calculated contours of $\log_{10} K_{eq}$ for impure garnet and ilmenite compositions. The Al_2SiO_5 phase relations from Holdaway (1971) and the α-quartz–β-quartz transition from Cohen and Klement (1967) are shown for reference. Note that slopes of the contours change slightly when they cross reaction boundaries, reflecting changes in the ΔV of the reaction. Mineral abbreviations: and = andalusite, alm = almandine, gt = garnet, ilm = ilmenite, ky = kyanite, qz = quartz, rut = rutile, sil = sillimanite. (After Bohlen *et al.*, 1983b, Fig.3, p.1054.)

Equilibrium coexistence of the GRAIL assemblage minerals is sometimes difficult to demonstrate because of the very low (commonly < 1%) modal abundance of the Ti-bearing oxides. Bohlen *et al.* (1983b) recommended using assemblages in which ilmenite and rutile are present as inclusions in garnet

and exhibit grain boundary relations indicative of chemical equilibrium.

An advantage of this geobarometer is the relatively less complicated calculation of its equilibrium constant. In natural GRAIL assemblages, compositions of three of the phases – quartz, rutile, and the Al_2SiO_5 polymorph – commonly differ little from the end-member components considered for reaction (6.9), so that their activities are equal to unity if the standard state of each phase is taken as the pure substance at the pressure and temperature of interest. Ilmenite in the GRAIL assemblage seldom contains more than 15% hematite (Fe_2O_3) and pyrophanite ($MnTiO_3$), and can be treated as an ideal solution or even as a pure phase in some cases. Thus, to a first approximation, the pressure inferred from a GRAIL assemblage in equilibrium is a function of the garnet composition (at constant temperature).

In order to calculate activities, Bohlen *et al.* (1983b) adopted the following symmetric ternary (Ca–Fe–Mg) mixing model for garnet (Perkins, 1979, as quoted in Bohlen *et al.*, 1983a):

$$RT \ln \lambda^{gt}_{alm} = W^G_{CaFe} X^2_{Ca} + W^G_{FeMg} X^2_{Mg} + (W^G_{CaFe} - W^G_{CaMg} + W^G_{FeMg}) X_{Ca} X_{Mg}$$

$$W^G_{FeMg} = 3480 - 1.2\,t\,(°C)\ \text{cal gm – atom}^{-1}$$

$$W^G_{CaFe} = 4180 - 1.2\,t\,(°C)\ \text{cal gm – atom}^{-1} \qquad (6.17)$$

$$W^G_{CaFe} = 1050 - 1.2\,t\,(°C)\ \text{cal gm – atom}^{-1}$$

$$a^{gt}_{alm} = (X_{Fe} \lambda^{gt}_{alm})^3$$

where W^Gs represent free-energy interaction parameters. The Perkins model, according to Bohlen *et al.* (1983b), is consistent with the bulk of the empirical data and yields pressures consistent with the appropriate Al_2SiO_5 mineral in the GRAIL assemblage. For garnets with significant Mn content, the authors assumed that Fe–Mn garnets mix ideally (Ganguly and Kennedy, 1974) and that $W^G_{CaMn} = W^G_{CaFe}$ and $W^G_{MgMn} = W^G_{MgFe}$.

Bohlen *et al.* (1983b) applied the GRAIL geobarometers to several metamorphic terranes and found the calculated pressures to be consistent with the appropriate Al_2SiO_5 polymorph(s) and generally in good agreement with other well-calibrated geobarometers.

Example 6–2: Application of GRAIL geobarometry to a sample from the Settler Schist, British Columbia, Canada

Let us estimate the equilibrium pressures for the Settler Schist corresponding to 600°C, using the analytical data of Pigage (1976), the solution model of Perkins (1979) for garnet, and the calibration of the GRAIL equilibrium by Bohlen *et al.* (1983b).

Electron microprobe analyses of minerals from the staurolite–kyanite–garnet–biotite–muscovite–quartz–plagioclase–ilmenite–rutile assemblage in the Settler Schist (Pigage, 1976) indicate that ilmenite and rutile are pure phases. Thus, taking the standard state as pure substances at the pressure and temperature of interest, and assuming kyanite and quartz to be a pure phases, $a^{qz}_{SiO_2} = 1$, $a^{ilm}_{FeTiO_3} = 1$, $a^{rut}_{TiO_2} = 1$, and $a^{ky}_{Al_2SiO_5} = 1$. Substituting the activity values in equation (6.15),

$$K_{eq} = \frac{1}{a^{gt}_{alm}} \qquad (6.18)$$

For the purpose of illustration, let us choose a typical composition of garnet in the Settler Schist: $(Mg_{0.4}Fe^{2+}_{2.15}Ca_{0.4}Mn_{0.05})Al_2Si_3O_{12}$. The calculated mole fractions for this composition are: $X_{Mg} = 0.133$, $X_{Fe^{2+}} = 0.717$, $X_{Ca} = 0.133$, and $X_{Mn} = 0.017$. Now we can calculate $a_{alm}{}^{gt}$ using equation (6.17) and K_{eq} using equation (6.18), and then obtain P from $\log_{10}K_{eq}$ contours in Fig. 6.5. The result, ignoring the very small contribution of Mn in the cpx solid solution, is summarized in Table 6.3.

The pressure calculated with the GRAIL geobarometer agrees well with the metamorphic conditions – 550 to 770°C and 6 to 8 kbar – inferred for the Settler Schist by Pigage (1976) using other methods.

6.4.3 *Garnet–plagioclase–pyroxene–quartz (GAPES and GADS) barometry*

Two of the potentially most useful geobarometers are based on the mineral assemblage garnet (gt)–plagioclase (plag)–orthopyroxene (opx) or clinopyroxene (cpx)–quartz (qz), which occurs widely in quartzofeldspathic and mafic lithologies of granulite metamorphic facies. The reactions considered for this purpose, commonly referred to as GAPES

Table 6.3 Results of the GRAIL geobarometry calculation for the Settler Schist.

Temperature (°C)	W^G_{FeMg}	W^G_{CaMg}	W^G_{CaFe}	$RT \ln \lambda^{gt}_{alm}$	λ^{gt}_{alm}	$a^{gt}_{alm} = (X_{Fe^{2+}} \lambda^{gt}_{alm})^3$	K_{eq}	$\log_{10}K_{eq}$	P (kbar)
600	2760	3460	330	47.999	1.205	0.646	2.494	0.397	≈ 6.2

W^Gs are in cal gm - atom^{-1}; R = 1.987 cal mol^{-1}K^{-1}.

(grossular–anorthite–pyrope–enstatite–silica) and GADS (garnet–anorthite–diopside–silica), are:

$$\underset{\text{anorthite (an)}}{\overset{\text{plag}}{CaAl_2Si_2O_8}} + \underset{\text{enstatite (en)}}{\overset{\text{opx}}{Mg_2Si_2O_6}} \Leftrightarrow \underset{\text{pyrope (py)}}{\overset{\text{gt}}{2/3Mg_3Al_2Si_3O_{12}}} + \underset{\text{grossular (gr)}}{\overset{\text{gt}}{1/3Ca_3Al_2Si_3O_{12}}} + \overset{\text{qz}}{SiO_2} \tag{6.19}$$

$$\underset{\text{anorthite (an)}}{\overset{\text{plag}}{CaAl_2Si_2O_8}} + \underset{\text{diopside (diop)}}{\overset{\text{opx}}{CaMgSi_2O_6}} \Leftrightarrow \underset{\text{pyrope (py)}}{\overset{\text{gt}}{1/3Mg_3Al_2Si_3O_{12}}} + \underset{\text{grossular (gr)}}{\overset{\text{gt}}{2/3Ca_3Al_2Si_3O_{12}}} + \overset{\text{qz}}{SiO_2} \tag{6.20}$$

These reactions are accompanied by large volume changes and thus are suitable, in principle, for geobarometry.

Experimental investigations of the two reactions at high temperature and high pressure have been hindered by apparent metastable persistence of anorthite + pyroxene assemblages, but the reactions were calibrated by Eckert *et al.* (1991) using measured values of the relevant thermodynamic parameters. For simplicity, let us assume that $(\Delta C_P)_r = 0$ (i.e., ΔH_r and ΔS_r are independent of temperature) and ΔV_r is independent of temperature and pressure. Choosing the standard state for each phase as the pure substance at P and T, the pressure and temperature of interest, and recognizing that $P >> 1$ bar, equation (6.13) reduces to

$$\Delta G^0_r = \Delta H^1_{r,T} - T\,\Delta S^1_{r,T} + P\,\Delta V_r = -RT \ln K_{eq} \tag{6.21}$$

Substituting values of ΔH^1_r, ΔS^1_r, and ΔV^1_r listed in Table 6.4, the thermobarometric equations, with uncertainties in the calculated P, are (Eckert *et al.*, 1991):

$$\text{GAPES:} \quad P\,(\text{kbars}) = 3.47 + 0.01307\,T + 0.003503\,T \ln K_{eq}\ (\pm 1.55\,\text{kbar}) \tag{6.22}$$

$$\text{GADS:} \quad P\,(\text{kbars}) = 2.60 + 0.01718\,T + 0.003596\,T \ln K_{eq}\ (\pm 1.90\,\text{kbar}) \tag{6.23}$$

To calculate P from equations (6.22) and (6.23) for a known or assumed value of T, we need to evaluate the corresponding values of K_{eq}:

$$K_{eq\,(GAPES)} = \frac{(a^{gt}_{py})^{\frac{2}{3}}(a^{gt}_{gr})^{\frac{1}{3}}\,a^{qz}_{SiO_2}}{a^{plag}_{an}\,a^{opx}_{en}} \tag{6.24}$$

$$K_{eq\,(GADS)} = \frac{(a^{gt}_{py})^{\frac{1}{3}}(a^{gt}_{gr})^{\frac{2}{3}}\,a^{qz}_{SiO_2}}{a^{plag}_{an}\,a^{cpx}_{diop}} \tag{6.25}$$

The activity of quartz, almost always a pure phase, was taken as unity. For the solid solutions in equation (6.19),

Table 6.4 Values used by Eckert et al. (1991) for calibration of GAPES and GADS geobarometers.

	ΔH^1_r (J)	ΔS^1_r (J K^{-1})	ΔV^1_r (J bar^{-1})
GAPES reaction	8230	−31.033	−2.373
GADS reaction	6020	−39.719	−2.312

Eckert *et al.* (1991) adopted the solution models discussed in Newton and Perkins (1982) and Perkins and Chipera (1985). The garnet was treated as a ternary (Ca–Fe–Mg) symmetric regular solution (Ganguly and Kennedy, 1974), with $W^G_{CaFe} \approx 0$, and the activity coefficients of the grossular and pyrope components in garnet solid solution were calculated using the following expressions:

$$\begin{aligned} RT \ln \lambda^{gt}_{Ca} &= W^G_{CaFe}X^2_{Fe} + W^G_{CaMg}X^2_{Mg} + (W^G_{CaFe} - W^G_{FeMg} + W^G_{CaMg})X_{Fe}X_{Mg} \\ &= W^G_{CaMg}\,(X^2_{Mg} + X_{Fe}X_{Mg}) \end{aligned} \tag{6.26}$$

$$\begin{aligned} RT \ln \lambda^{gt}_{Mg} &= W^G_{FeMg}\,X^2_{Fe} + W^G_{CaMg}\,X^2_{Ca} + (W^G_{FeMg} - W^G_{CaFe} + W^G_{CaMg})\,X_{Fe}X_{Ca} \\ &= W^G_{CaMg}\,(X^2_{Ca} + X_{Fe}X_{Ca}) \end{aligned}$$

Assuming no mixing on the octahedral and tetrahedral sites and taking into account the three positions of Ca–Fe–Mg mixing on the cubic site in the formula unit of garnet (12 O atoms basis),

$$a^{gt}_{py} = (X_{Mg}\lambda_{Mg})^3 = X^3_{Mg}\left\{\exp\left[\frac{W^G_{CaMg}}{RT}(X^2_{Ca} + X_{Ca}X_{Fe})\right]\right\}^3 \tag{6.27}$$

$$a^{gt}_{gr} = (X_{Ca}\lambda_{Ca})^3 = X^3_{Ca}\left\{\exp\left[\frac{W^G_{CaMg}}{RT}(X^2_{Ca} + X_{Mg}X_{Fe})\right]\right\}^3 \tag{6.28}$$

where $W^G_{CaMg} = 13807 - 6.3T$ J mol^{-1} (four O atoms basis), and $R = 8.314$ J mol^{-1} K^{-1}.

Expressions used for calculating the activities of enstatite and diopside components in pyroxene on the basis of an ideal two-site MOS (mixing-on-site) model were adopted from Wood and Banno (1973):

$$a^{opx}_{en} = X^{M2}_{Mg}\,X^{M1}_{Mg} \tag{6.29}$$

$$a^{cpx}_{diop} = X^{M2}_{Ca}\,X^{M1}_{Mg} \tag{6.30}$$

The cation assignments for calculation of mole fractions in clinopyroxene were as follows: Ca, Na, Mn, and Fe^{2+} to $M2$; and Mg, Ti, Fe^{3+}, Al^{VI}, and remaining Fe^{2+} to $M1$. The cation assignments were the same for orthopyroxene, except that Fe^{2+} and Mg were considered to be distributed randomly

between *M*1 and *M*2 sites and partitioned between the two sites such that

$$\left(\frac{\text{Mg}}{\text{Mg}+\text{Fe}^{2+}}\right)^{M1} = \left(\frac{\text{Mg}}{\text{Mg}+\text{Fe}^{2+}}\right)^{M2} = \left(\frac{\text{Mg}}{\text{Mg}+\text{Fe}^{2+}}\right)^{\text{mineral}} \tag{6.31}$$

The above formulation assumes that there is no mixing on the tetrahedral positions.

The calculation of the activity coefficient of the anorthite component in plagioclase (λ_{an}^{plag}) was based on the "Al-avoidance" model of Kerrick and Darken (1975): that

$$RT \ln \lambda_{an}^{plag} = X_{ab}^2[W_{an}^G + 2X_{an}(W_{ab}^G - W_{an}^G)] \tag{6.32}$$

where $W_{an}^G = 2025\,\text{cal} = 8473\,\text{J}$ and $W_{ab}^G = 6746\,\text{cal} = 28225\,\text{J}$ (Newton *et al*., 1980). The activity coefficient multiplied with the activity of anorthite in an ideal plagioclase solid solution (equation 5.88) led to the following expression for a_{an}^{plag}

$$\begin{aligned} a_{an}^{plag} &= \frac{X_{an}(1+X_{an})^2}{4}\lambda_{an}^{plag} \\ &= \frac{X_{an}(1+X_{an})^2}{4}\exp\left[\frac{X_{ab}^2(8473+39505X_{an})}{RT}\right] \end{aligned} \tag{6.33}$$

Eckert *et al*. (1992) calculated GAPES and GADS pressures for a granulite-facies core of Paleozoic metamorphism in the Blue Ridge province of the North Carolina Appalachians, at an inferred temperature of 750°C, using five different formulations for each barometer. The calculated GAPES pressures (7.2 to 8.9 kbars) showed reasonable to good agreement, all falling in the sillimanite field of the experimental Al_2SiO_5 phase diagram, consistent with the location of the samples relative to mapped kyanite and sillimanite isograds in the area and with the presence of peak-metamorphic sillimanite in nearby metapelites. The calculated GADS pressures agreed reasonably well with the GAPES pressures from the same rock or adjacent outcrops, but were systematically higher by 130–590 bars, suggesting that an empirical pressure adjustment of −350 bars to the GADS calculations would be necessary to force an agreement between the two geobarometers.

6.5 Exchange reactions

Exchange reactions are heterogeneous reactions that are written only in terms of the exchange of two similar cations (in respect of ionic radius and charge) between nonequivalent atomic sites in one mineral (*intracrystalline exchange*) or between atomic sites in two different coexisting minerals (*intercrystalline exchange*). Exchange reactions are accompanied by very small volume changes but relatively large entropy changes, so that they are largely independent of pressure and potentially good geothermometers (Essene, 1982). However, intracrystalline exchange, such as of Fe^{2+}–Mg^{2+} between *M*1 and *M*2 sites in orthopyroxene,

$$Fe^{2+}\,(M2) + Mg^{2+}\,(M1) = Fe^{2+}\,(M1) + Mg^{2+}\,(M2) \tag{6.34}$$

requires diffusion of Fe^{2+} and Mg^{2+} to be operative over very short distances, which makes the cation distribution prone to resetting. In general, intercrystalline cation distributions are relatively less vulnerable to resetting, as the diffusion has to occur over much larger distances.

The general form of an intercrystalline exchange equilibrium involving 1 mole each of two elements (or cations) *A* and *B* between the phases α and β may be written as

$$A\,(\alpha) + B\,(\beta) \Leftrightarrow A\,(\beta) + B\,(\alpha) \tag{6.35}$$

The equilibrium constant for the reaction at *P* and *T* is

$$\begin{aligned} K_{eq}(P,T) &= \frac{(a_A)^\beta\,(a_B)^\alpha}{(a_A)^\alpha\,(a_B)^\beta} = \frac{(X_A)^\beta\,(X_B)^\alpha}{(X_A)^\alpha\,(X_B)^\beta}\cdot\frac{(\lambda_A)^\beta\,(\lambda_B)^\alpha}{(\lambda_A)^\alpha\,(\lambda_B)^\beta} \\ &= \frac{(X_A/X_B)^\alpha}{(X_A/X_B)^\beta}\cdot\frac{(\lambda_A/\lambda_B)^\alpha}{(\lambda_A/\lambda_B)^\beta} \end{aligned} \tag{6.36}$$

where a_i, X_i, and λ_i represent, respectively, the activity, mole fraction, and rational activity coefficient of the constituent *i*. Denoting the ratio of mole fractions in equation (6.36) as K_D, the *empirical distribution coefficient* for the exchange (see section 3.7.2), and the ratio of activity coefficients as K_λ, then

$$K_{eq}(P,T) = K_D\,K_\lambda(P,T) \tag{6.37}$$

where K_λ is a function of *P* and *T*. Note that if α and β are ideal solutions, then $\lambda_i = 1$ and $K_{eq}(P,T) = K_D(P,T)$. In this case, a plot of $(X_A/X_B)^\alpha$ versus $(X_A/X_B)^\beta$ for a suite of rocks that equilibrated at the same temperature and pressure should define a straight line with a slope equal to K_D. As a general rule, the preference of a phase to exchange one element for another decreases with increasing temperature and K_D approaches a value of 1. This is because as temperature is increased, the energetic distinction between different elements becomes relatively smaller, so the crystal structures display less of a preference for one element over another (Spear, 1993).

Choosing the standard state of each phase as a pure substance at the *P* and *T* of interest, and assuming $(\Delta C_p)_r = 0$, ΔV_r (solids) to be independent of temperature and pressure, and $P \gg 1$ bar, we have (see equation 6.21)

$$-RT \ln K_{eq}(P,T) = \Delta H^1_{r,T} - T\,\Delta S^1_{r,T} + P\,\Delta V_r \tag{6.38}$$

Application of this relationship to geothermometry requires the calibration of K_{eq} as a function of T for known or assumed values of P.

Many exchange geothermometers have been discussed in the literature, but here we will restrict our attention to Fe^{2+}–Mg^{2+} exchange reactions, the most widely applied thermometers in metamorphic rocks. This is because Fe^{2+}–Mg^{2+} substitute easily for each other in many common metamorphic minerals and the relatively high concentrations of Fe^{2+}–Mg^{2+} in these minerals permit their precise measurement with an electron microprobe. Microprobe analysis, however, measures the total Fe in a mineral, which then has to be recast into Fe^3 and Fe^2 by some established procedure.

6.5.1 Garnet–clinopyroxene thermometry

The temperature dependence of Fe^{2+}–Mg^{2+} exchange between the minerals garnet and clinopyroxene has long since been recognized as an important potential geothermometer, because the assemblage is common in amphibolites, granulites, and eclogites that span a broad temperature range. It is probably the most useful and consistent of the Fe–Mg exchange thermometers for high-grade metamorphic terranes (Pattison and Newton, 1989) and is particularly applicable to low-Na and low-Cr mineral compositions that are typical of eclogites and granulites. The pertinent exchange reaction in terms of end-member components is

$$\underset{\text{pyrope (py)}}{1/3\overset{gt}{Mg_3Al_2Si_3O_{12}}} + \underset{\text{hedenbergite (hd)}}{\overset{cpx}{CaFeSi_2O_6}} \Leftrightarrow \underset{\text{almandine (alm)}}{1/3\overset{gt}{Fe_3Al_2Si_3O_{12}}} + \underset{\text{diopside (diop)}}{\overset{cpx}{CaMgSi_2O_6}} \quad (6.39)$$

Taking into account the three positions for Fe–Mg mixing in the garnet (12 O atom basis) and only one position of Fe–Mg mixing in the clinopyroxene, the equilibrium constant of the reaction is:

$$\begin{aligned} K_{eq} &= \frac{(a^{gt}_{alm})^{\frac{1}{3}}\, a^{cpx}_{diop}}{(a^{gt}_{py})^{\frac{1}{3}}\, a^{cpx}_{hd}} = \frac{X^{gt}_{Fe}\, X^{cpx}_{Mg}}{X^{cpx}_{Fe}\, X^{gt}_{Mg}}\ \frac{\lambda^{gt}_{Fe}\, \lambda^{cpx}_{Mg}}{\lambda^{cpx}_{Fe}\, \lambda^{gt}_{Mg}} \\ &= \frac{\left(X_{Fe}/X_{Mg}\right)^{gt}}{\left(X_{Fe}/X_{Mg}\right)^{cpx}}\ \frac{\left(\lambda_{Fe}/\lambda_{Mg}\right)^{gt}}{\left(\lambda_{Fe}/\lambda_{Mg}\right)^{cpx}} = K_D\ K_\lambda \end{aligned} \quad (6.40)$$

Several authors have proposed equations relating T to K_{eq} (Table 6.5), which can be used to calculate T from the compositions of coexisting garnet and clinopyroxene if P is estimated from some other source. The empirical calibration of Dahl

Table 6.5 Some explicit equations proposed for garnet–clinopyroxene geothermometry

Author(s)	Data for calibration	Equation for T (K) (P in kbar)	
Råheim and Green (1974)	Experimental	$\dfrac{3686 + 28.35\,P}{\ln K_D + 2.33}$	(6.41)
Ellis and Green (1979)	Experimental	$\dfrac{3104\,(X^{gt}_{Ca}) + 3030 + 10.86\,P}{\ln K_D + 1.9034}$	(6.42)
Dahl (1980)	Empirical (based on a granulite terrane)	$\dfrac{2482 + 1509(X^{gt}_{Fe} - X^{gt}_{Mg}) + 2810(X^{gt}_{Ca}) + 2855(X^{gt}_{Mn})}{R \ln K_D}$	(6.43)
Krogh (1988)	Reinterpretation of existing experimental data	$\dfrac{-6137\,(X^{gt}_{Ca})^2 + 6731\,(X^{gt}_{Ca}) + 1879 + 10\,P}{\ln K_D + 1.393}$	(6.44)
Pattison and Newton (1989)	Experimental	$\dfrac{a'X^3 + b'X^2 + c'X + d'}{\ln K_D + a_oX^3 + b_oX^2 + c_oX + d_o} + 5.5\,(P - 15)$; where a_o, b_o, c_o, d_o, a′, b′, c′, and d′ are parameters determined from experimental data	(6.45)
Ai (1994)	Experimental	$\dfrac{[-1629(X^{gt}_{Ca})^2 + 3648.55(X^{gt}_{Ca}) - 6.59\,\{\text{mg \# (gt)}\} + 1987.98 + 17.66P]}{\ln K_D + 1.076}$	(6.46)

mg# (magnesium number) = [molar Mg/(Mg + Fe)]100. The uncertainties in the temperatures estimated by these geothermometers are generally ±5% in the 800°–1200°C range, but may be somewhat larger toward the low temperature end of this range because of the lack of extensive experimental data or well-constrained thermochemical parameters at such temperatures.

(1980) (equation 6.43) gives widely scattered, erratic results and is not reliable. The experimental calibration of Råheim and Green (1974) (equation 6.41) was based on a series of natural basaltic rocks [Mg/(Mg + Fe) = 0.062–0.85] crystallized to eclogite at 20–40 kbar and 600°–1400°C. In order to test the effects of variations in the compositions (Na, Ca) of clinopyroxene and garnet on K_D, Ellis and Green (1979) obtained additional experimental data on a series of basaltic compositions in the range of 24–30 kbar and 750°–1300°C. The variation of K_D over a wide range of pressure, temperature, and rock composition was found to be a function of X^{gt}_{Ca} [where X^{gt}_{Ca} = Ca/(Ca + Mg + Fe^{2+} + Mn)] at any given *P, T* condition and could be accounted for by the linear relationship

$$\ln K_D = c\, X^{gt}_{Ca} + d$$

where the constants *c* and *d*, which incorporate the total non-ideal effects on K_D, were determined from the experimental data (equation 6.42). Using experimental data available at the time, Krogh (1988) proposed a new equation (equation 6.44), which replaced the linear relationship between X_{Ca}(gt) and ln K_D by a curvilinear relationship. Application of this calibration to a suite of samples of eclogites and associated omphacite–garnet-bearing gneisses showed that the calculated temperatures did not vary much with rather large variations in the Mg:(Mg + Fe) ratio of the garnet (0.17–0.54) and Na content of the clinopyroxene (0.11–0.44).

Pattison and Newton (1989) showed from experimental study that the magnesium number (mg #) of garnet had a significant effect on K_D. They fitted their experimental data on synthetic compositions (mg # 12.5 to 60) to a third-order polynomial,

$$\ln K_D = aY^3 + bY^2 + cY + d$$

where *Y* represents the Mg:(Mg + Fe) ratio of the garnet and the coefficients are functions of 1/*T* (e.g., $a = a_o + a_1(1/T)$, etc.), an apparent contradiction with the experimental observation of Råheim and Green (1974) that K_D increases with increasing temperature. The geothermometer (equation 6.45) requires the extraction of eight parameters (or coefficients) for each garnet composition and, as the authors have cautioned, it should not be applied outside the experimental range of garnet composition, X^{gt}_{Ca} = 0.125 – 0.600. Overall, temperatures calculated using equation (6.45) are 0 to 60°C lower than those obtained by Råheim and Green (1974) and 60° to150°C lower than those of Ellis and Green (1979). For high-pressure mantle rocks (*T* greater than about 1000° C) temperatures calculated with the calibration of Ai (1994) (equation 6.46), based on all the experimental data available at the time, are similar to those of Ellis and Green (1979), but may be lower by as much as about 100°C for crustal rocks.

Berman *et al.* (1995) proposed a "provisional" solution model to evaluate ln K_λ for the calibration of the garnet–clinopyroxene geothermometer. For this model, the *M*1 site in clinopyroxene is treated as a symmetric ternary regular solution of Mg, Fe, and Al atoms, and the *M*2 site as a quaternary solution of Na, Ca, Fe and Mg atoms; Mg:(Mg + Fe) is assumed to be equal in both *M*1 and *M*2. The garnet is considered to be a Ca–Mg–Fe ternary solution, with each of the three binary joins modeled as asymmetric regular solution.

The geothermometer of Ellis and Green (1979) is the one that is most commonly used for intermediate, mafic, and ultramafic rocks from metamorphic terranes and from xenolith assemblages as it agrees more closely with feldspar- and oxide-based temperature determinations than other formulations. From a comparison of the various formulations of the garnet–clinopyroxene thermometer, Green and Adam (1991) concluded that the Ellis and Green (1979) calibration may result in an overestimation of temperature when applied to crustal rocks formed at low to moderate pressures (10–20 kbar), but temperatures for such rocks calculated using the solution model of Berman *et al.* (1995) are quite similar to that produced with the formulation by Ellis and Green (1979).

6.5.2 *Garnet–biotite (GABI) thermometry*

The garnet (gt)–biotite (bi) Fe–Mg exchange geothermometer is one of the most widely used geothermometers for estimating the temperature of equilibration of medium- and high-grade metamorphic rocks. The cation exchange equilibrium can be expressed in terms of end-member components of garnet and biotite as:

garnet biotite garnet biotite

$$Fe_3Al_2Si_3O_{12} + KMg_3AlSi_3O_{10}(OH)_2 \Leftrightarrow Mg_3Al_2Si_3O_{12} + KFe_3AlSi_3O_{10}(OH)_2 \qquad (6.47)$$

almandine phlogopite pyrope annite

The equilibrium constant of the reaction, taking into account the Fe–Mg exchange on three crystallographic sites, is:

$$K_{eq} = \frac{\left(X^{gt}_{Mg}\right)^3 \Big/ \left(X^{gt}_{Fe}\right)^3}{\left(X^{bi}_{Mg}\right)^3 \Big/ \left(X^{bi}_{Fe}\right)^3} \cdot \frac{\left(\lambda^{gt}_{Mg}\right)^3 \Big/ \left(\lambda^{gt}_{Fe}\right)^3}{\left(\lambda^{bi}_{Mg}\right)^3 \Big/ \left(\lambda^{bi}_{Fe}\right)^3} = (K_D\ K_\lambda)^3 \qquad (6.48)$$

If ΔH_r and ΔS_r for reaction (6.47) are assumed to be independent of temperature and ΔV_r independent of temperature and pressure, we can combine equations (6.38) and (6.48) to get the following (see Box 6.2):

$$\ln\left(K_D\ K_\lambda\right)(P,T) = \frac{1}{T}\left[\frac{-\left(\Delta H^1_{r,\,298.15} + P\,\Delta V_r\right)}{3R}\right] + \frac{\Delta S^1_{r,\,298.15}}{3R} \qquad (6.49)$$

Conducting reversed experiments for calibration of the partitioning of Fe and Mg between a large amount of synthetic Fe–Mg garnet of known composition and a small amount of

Box 6.2 Derivation of equation (6.49) for GABI thermometry

Separating the mole fractions term from the activity coefficients term in equation (6.48),

$K_{eq} = (K_D\, K_\lambda)^3$

$\ln K_{eq} = 3 \ln (K_D\, K_\lambda)$

where

$$K_D = \frac{\left(X_{Mg}^{gt}\right)/\left(X_{Fe}^{gt}\right)}{\left(X_{Mg}^{bi}\right)/\left(X_{Fe}^{bi}\right)} \quad \text{and} \quad K_\lambda = \frac{\left(\lambda_{Mg}^{gt}\right)/\left(\lambda_{Fe}^{gt}\right)}{\left(\lambda_{Mg}^{bi}\right)/\left(\lambda_{Fe}^{bi}\right)}$$

Substituting for K_{eq} in equation (6.38),

$$-RT \ln K_{eq}(P, T) = \Delta H^1_{r,T} - T\,\Delta S^1_{r,T} + P\,\Delta V_r$$

$$-3RT \ln (K_D\, K_\lambda)\,(P, T) = \Delta H^1_{r,T} - T\,\Delta S^1_{r,T} + P\,\Delta V_r$$

$$\ln (K_D\, K_\lambda)\,(P, T) = \frac{-\Delta H^1_{r,T} - T\,\Delta S^1_{r,T} + P\,\Delta V_r}{3RT}$$

which can be rearranged to give equation (6.49)

$$\ln \left(K_D\, K_\lambda\right)(P,T) = \frac{1}{T}\left[\frac{-\left(\Delta H^1_{r,298.15} + P\,\Delta V_r\right)}{3R}\right] + \frac{\Delta S^1_{r,298.15}}{3R} \qquad (6.49)$$

Fe–Mg biotite of unknown composition at temperatures ranging from 550 to 800°C, Ferry and Spear (1978) established the relation between K_D and T (at P = 2.07 kbar, the pressure at which the experiment was conducted) as:

$$\ln KD = -2109/T(K) + 0.782 \qquad (6.50)$$

where $K_D = (Mg/Fe)_{gr}/(Mg/Fe)_{bi}$ (either on a weight or atomic basis). This equation is consistent with ideal mixing of Fe and Mg in biotite and garnet solid solutions (i.e., $a_i = X_i$ so that K_λ = 1 in equation (6.49)), at least in the compositional range studied in their experiments ($0.80 \le Fe/(Fe + Mg) \le 1.00$). The coefficients in this equation were determined by a linear least-squares fit of the experimental values of $\ln K_D$ versus $1/T$ (Fig. 6.6). The straight-line plot in Fig. 6.7 indicates that the assumptions $-\Delta C_r^0 = 0$ and $\Delta V_r = 0$ – are quite reasonable. Comparing equation (6.49) with equation (6.50), and substituting $\Delta V_r = 0.057$ cal bar^{-1} = 0.238 J bar^{-1} (using molar volume data at 298.15 K and 1 bar from Robie *et al.*, 1978), they determined that at P = 2070 bars (the pressure at which the experiment was conducted),

$$\Delta S^1_{r,298.15} = 3R\,(0.782) = 4.662\ \text{cal K}^{-1} = 19.51\ \text{J K}^{-1}$$

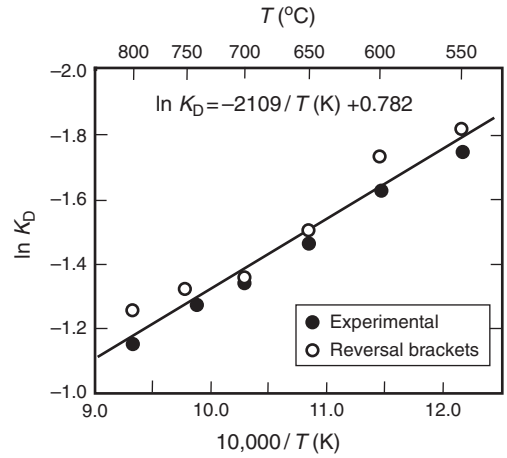

Fig. 6.6 Plot of $\ln K_D$[= $\ln \{(Mg/Fe)_{garnet}/(Mg/Fe)\}_{biotite}$] versus 1/T (K) for experimentally equilibrated garnet–biotite pairs by Ferry and Spear (1978). The solid circle–open circle pairs represent reversal brackets, and the solid line the calculated least-squares fit to the data points. (After Ferry and Spear, 1978, Figure 3, p.115.)

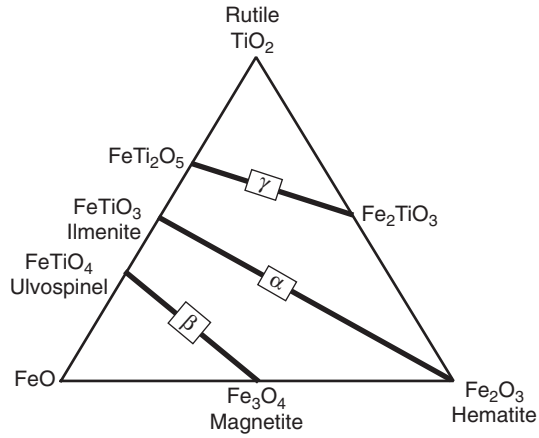

Fig. 6.7 The major solid solution series of the FeO–Fe_2O_3–TiO_2 system: ilmenite ($FeTiO_3$)–hematite (Fe_2O_3) solid solution [α phase, rhombohedral]; magnetite (Fe_3O_4)–ulvöspinel (Fe_2TiO_4) solid solution [β phase, cubic]; and ferropseudobrookite ($FeTi_2O_5$)–pseudobrookite (Fe_2TiO_5) solid solution [γ phase, orthorhombic]. Compositions are in mole percent.

$$\Delta H^1_{r,298.15} = 3R\,(2109) - 2070\,(\Delta V_r) = 12{,}454\ \text{cal} = 52{,}108\ \text{J}$$

Substituting the above values in equation (6.49) (and assuming $K_\lambda = 1$),

$$52{,}108\ (\text{J}) - 19.51\ T\ (\text{K}) + 0.238\ P\ (\text{bars}) + 3RT \ln K_D = 0 \qquad (6.51)$$

which can be rearranged as (R = 8.314 J mol^{-1} K^{-1}):

$$\ln K_D = -(2089 + 0.0096P)/T + 0.782 \qquad (6.52)$$

Note that the effect of pressure on this exchange equilibrium is small (as it should be for a good geothermometer) so that the error introduced on account of uncertainty in the estimated pressure will be small. This reaction is appropriate for geothermometry because of the relatively large ΔH_r and quite small ΔV_r.

Equation (6.52) can be used to calculate T for a given rock first by calculating K_D from electron microprobe analysis of coexisting garnet and biotite, and then obtaining an independent estimate of P, provided that the garnet and biotite compositions lie close to the Mg–Fe binary and the Mg–Fe mixing is ideal in both the minerals. In reality, the activity–composition relations are more complicated because of dilution of the solid solutions – with Ca and Mn in garnets, and with Al^{VI} and Ti in biotites – and the nonideality of the solutions. In addition, natural and synthetic biotites and garnets contain Fe^{3+}, which was not been taken into account in the calibration of Ferry and Spear (1978). They considered it a useful thermometer (with a maximum practical resolution of approximately ±50°C) without correction for components other than Fe and Mg [(Ca + Mn)/(Ca + Mn + Fe + Mg) up to ~0.2 in garnet and (Al^{VI} + Ti)/(Al^{VI} + Ti + Fe + Mg) up to ~0.15 in biotite].

Over the past two decades, a number of calibrations of the GABI geothermometer, incorporating different mixing models for garnet or biotite or both, have been discussed in the literature (see Table 6.1). Holdaway (2000) made a statistical comparison of several of these models and concluded that the models of Berman and Aranovich (1996), Ganguly *et al.* (1996), and Mukhopadhyay *et al.* (1997) can be used to produce reasonable garnet–biotite geothermometer calibrations.

6.5.3 *Magnetite–ilmenite thermometry and oxygen barometry*

The compositions of coexisting magnetite–ulvöspinel solid solution (mt_{ss} or β phase; cubic) and ilmenite–hematite solid solution (ilm_{ss} or α phase; rhombohedral) (Fig. 6.7), the two most common iron–titanium oxide minerals in rocks and mineral deposits, provide information about not only the temperature of equilibration but also the corresponding oxygen fugacity. The method is best suited to extrusive and hypabyssal igneous rocks that were subjected to relatively rapid cooling and are unmetamorphosed. Its application to plutonic igneous rocks and mineral deposits should be viewed with caution because of likely reequilibration subsequent to crystallization.

The crystal structure of both hematite ($Fe_2^{2+}O_3$) and ilmenite ($Fe^{2+}Ti^{4+}O_3$) may be described as a hexagonal close-packed array of oxygen atoms with octahedrally coordinated metal atoms in the interstices. In pure ilmenite, there are two cation sites, one (site A) containing Fe^{2+} and the other (site B) containing Ti^{4+}. In pure hematite the two sites are indistinguishable as both contain only Fe^{2+}. In the structure of the ilm_{ss}, Ti is assumed to be restricted to the B sites, as in pure ilmenite, where it mixes randomly with Fe^{3+}, and Fe^{2+} is restricted to the A sites where it mixes randomly with the rest of Fe^{3+} (Rumble, 1977). For the pure Fe–Ti–O system, a further constraint in this model is that the amount of Fe^{2+} and Fe^{3+} on the A and B sites must be equal in order to preserve charge balance. Thus, we may accept a structural model for ilm_{ss} that is ordered in terms of A and B sites but disordered in respect of Fe^{3+}.

In spinels ($A^{IV}B_2{}^{VI}O_4$) with "normal" structure, A cations occupy the tetrahedral sites and B cations only the octahedral sites. But both magnetite (Fe_3O_4) and ulvöspinel (Fe_2TiO_4) have "inverse" spinel structure – that is, one-half of the B cations occupy tetrahedral sites, and the other half of the B cations and the A cations occupy octahedral sites – and their structural formulas may be written as $(Fe^{3+})^{IV}[Fe^{2+}\ Fe^{3+}]^{VI}O_4$ and $(Fe^{2+})^{IV}[Fe^{2+}\ Ti^{4+}]^{VI}O_4$. Several models have been proposed to account for the cation distribution in mt_{ss}, and the activity–composition relationships vary depending on the model adopted.

Thermodynamic equilibrium between mt_{ss} and ilm_{ss} may be represented by the reaction among the end-member components as

$$\underset{\beta\text{ phase}}{\left[y\mathrm{Fe_2TiO_4}+(1-y)\mathrm{Fe_3O_4}\right]}+\tfrac{1}{4}\mathrm{O_2}\Leftrightarrow\underset{\alpha\text{ phase}}{\left[y\mathrm{FeTiO_3}+\left(\tfrac{3}{2}-y\right)\mathrm{Fe_2O_3}\right]} \tag{6.53}$$

$$K_{eq}=\frac{\left(a^{\alpha}_{FeTiO_3}\right)^{y}\left(a^{\alpha}_{Fe_2O_3}\right)^{\frac{3}{2}-y}}{\left(a^{\beta}_{Fe_2TiO_4}\right)^{y}\left(a^{\beta}_{Fe_3O_4}\right)^{1-y}\left(f_{O_2}\right)^{\frac{1}{4}}} \tag{6.54}$$

As K_{eq} is a constant at given P, T and the effect of total pressure on this equilibrium is negligible (Buddington and Lindsley 1964), K_{eq} is essentially a function of temperature and f_{O_2}. Thus, the equilibrium temperature of the reaction and its associated f_{O_2} are defined simultaneously if the activities of all the solids are fixed. Buddington and Lindsley (1964) experimentally determined calibration curves for various compositions of the two solid solutions as a function of temperature and f_{O_2}, which could then be used to determine temperature and f_{O_2} for coexisting mt_{ss} and ilm_{ss} in equilibrium in natural assemblages. The calibration has subsequently been refined incorporating additional experimental data and solution models.

For thermodynamic modeling, the compositions of coexisting mt_{ss} and ilm_{ss} phases are considered in terms of two separate reactions involving end-member components:

(1) a Fe-Ti exchange reaction,

$$\underset{ilm}{\mathrm{FeTiO_3}}+\underset{mt}{\mathrm{Fe_3O_4}}\Leftrightarrow\underset{usp}{\mathrm{Fe_2TiO_4}}+\underset{hem}{\mathrm{Fe_2O_3}} \tag{6.55}$$

Since $\Delta G_r^0 = -RT \ln K_{eq}$ (equation 5.37),

$$-\frac{\Delta G^0_{exch}}{RT}=\ln K_{eq}=\ln\frac{\left(a^{mt_{ss}}_{usp}\right)^{\phi=1}\left(a^{ilm_{ss}}_{hem}\right)^{\phi=2}}{\left(a^{mt_{ss}}_{mt}\right)^{\phi=1}\left(a^{ilm_{ss}}_{ilm}\right)^{\phi=2}}$$
$$=\ln\frac{\left(X^{mt_{ss}}_{usp}\right)^{\phi=1}\left(X^{ilm_{ss}}_{hem}\right)^{\phi=2}}{\left(X^{mt_{ss}}_{mt}\right)^{\phi=1}\left(X^{ilm_{ss}}_{ilm}\right)^{\phi=2}}+\ln\frac{\left(\lambda^{mt\ ss}_{usp}\right)^{\phi=1}\left(\lambda^{ilm\ ss}_{hem}\right)^{\phi=2}}{\left(\lambda^{mt\ ss}_{mt}\right)^{\phi=1}\left(\lambda^{ilm\ ss}_{ilm}\right)^{\phi=2}} \tag{6.56}$$

(2) an oxidation reaction (oxidation of magnetite to hematite),

$$\underset{\text{mt}}{4\text{Fe}_3\text{O}_4}{}^{\text{mt}_{ss}} \Leftrightarrow \underset{\text{hem}}{6\text{Fe}_2\text{O}_3}{}^{\text{ilm}_{ss}} \tag{6.57}$$

$$\begin{aligned} -\frac{\Delta G^0_{\text{oxid}}}{RT} = \ln K_{\text{eq}} &= \ln \frac{\left(a^{\text{ilm ss}}_{\text{hem}}\right)^{6\,.\,\phi=2}}{\left(a^{\text{mt ss}}_{\text{mt}}\right)^{4.\,\phi=1} f_{\text{O}_2}} \\ &= \ln \frac{\left(X^{\text{ilm ss}}_{\text{hem}}\right)^{6\,.\,\phi=2}}{\left(X^{\text{mt ss}}_{\text{mt}}\right)^{4\,.\,\phi=1}} + \ln \frac{\left(\lambda^{\text{ilm ss}}_{\text{hem}}\right)^{6\,.\,\phi=2}}{\left(\lambda^{\text{mt ss}}_{\text{mt}}\right)^{4\,.\,\phi=1}} - \ln f_{\text{O}_2} \end{aligned} \tag{6.58}$$

The variable ϕ in equations (6.56) and (6.58) is set to 2 for ilm_{ss} and to 1 for mt_{ss} in accordance with configurational entropy expressions (Rumble, 1977). Spencer and Lindsley (1981) used the above reactions to revise the calibration of Buddington and Lindsley (1964) with a solution model based on least squares fit of thermodynamic parameters to experimental data in the range 550–1200°C obtained by various workers. The assumptions for the model are as follows: (i) ilm_{ss} behaves as a binary asymmetric regular solution; (ii) mt_{ss} behaves as a binary asymmetric regular solution below 800°C and as a binary ideal solution above 800°C; (iii) the activities of the components can be approximated by a molecular mixing model for the mt_{ss} (with the proportions of the different end-member "molecules" calculated in a specified sequence) and by disorder of Fe^{3+} in ilm_{ss}. The equations derived by them for calculation of the temperature and f_{O_2} of equilibration of a mt_{ss}–ilm_{ss} pair are:

$$T\ (\text{K}) = \frac{-\text{A}_1 W^H_{\text{usp}} - \text{A}_2 W^H_{\text{mt}} + \text{A}_3 W^H_{\text{ilm}} + \text{A}_4 W^H_{\text{hem}} + \Delta H^0_{\text{exch}}}{-\text{A}_1 W^S_{\text{usp}} - \text{A}_2 W^S_{\text{mt}} + \text{A}_3 W^S_{\text{ilm}} + \text{A}_4 W^S_{\text{hem}} + \Delta S^0_{\text{exch}} - R \ln K_{\text{exch}}} \tag{6.59}$$

$$\log f_{\text{O}_2} = \log \text{MH} + \frac{1}{2.303}\left[\frac{1}{RT}\begin{Bmatrix} 12 \ln (1 - X_{\text{ilm}}) - 4 \ln(1 - X_{\text{usp}}) + \\ 8X^2_{\text{usp}}\left(X_{\text{usp}} - 1\right)W^G_{\text{usp}} + 4X^2_{\text{usp}}\left(1 - 2X_{\text{usp}}\right)W^G_{\text{mt}} \\ +12X^2_{\text{ilm}}\left(1 - X_{\text{ilm}}\right)W^G_{\text{ilm}} - 6X^2_{\text{ilm}}\left(1 - 2X_{\text{ilm}}\right)W^G_{\text{hem}} \end{Bmatrix}\right] \tag{6.60}$$

where W^H and W^G are enthalpy and free-energy interaction parameters, respectively, and log MH is the value of $\log f_{\text{O}_2}$ of coexisting mt_{ss}–ilm_{ss} at T and is calculated as log MH = 13.996 – 24634/T.

The parameters for this model are listed in Table 6.6. Spencer and Lindsley (1981) suggested using the low-T parameters to calculate an initial temperature, and recalculating T by setting W^Gs = 0 for mt and usp (i.e., considering mt_{ss} to be ideal) if the initial temperature turned out to be greater than 800°C. Uncertainties in T and f_{O_2} according to the authors are approximately 40–80°C and 0.5–1.0 log units f_{O_2} (2σ), assuming 1% uncertainties in mt_{ss} and ilm_{ss} compositions. The T– f_{O_2} curves calculated from this model are shown in Fig. 6.8.

The calibration of Spencer and Lindsley (1981), like that of Buddington and Lindsley (1964), did not consider minor constituents (such as Mg, Mn, Ca, Al, Cr, V, Si, etc.) that may occur in the solid solutions due to ionic substitutions. Stormer (1983) recommended a scheme for calculation of what he called "apparent mole fractions" of the solid solution components that considered the effect of ionic substitutions while being consistent with the solution models of Spencer and Lindsley (1981). This scheme assumes that in ilm_{ss} the 2+ ions are confined to the A site with Fe^{2+}, the 4+ cations occupy the B sites with Ti^{4+}, and the 3+ cations and Fe^{3+} are randomly mixed in equal proportions on both sites. For mt_{ss} it is assumed that all the 4+ cations substitute for Ti^{4+} on the B sites, the two octahedral sites always contain one Fe^{2+} per formula unit, Fe^{2+} and Fe^{3+} substitute on the tetrahedral sites in ratios equal to the molar ratio of usp to mt, and the local charge balance is maintained by the substitution of 2+ cations for Fe^{2+} and of 3+ cations for Fe^{3+}. Incorporation of this scheme into the solution model of Spencer and Lindsley (1981) simply requires replacing the mole fractions (X_{ilm}, X_{hem}, X_{usp}, X_{mt}) used in equations (6.59) and (6.60) by corresponding apparent mole fractions (X^*_{ilm}, X^*_{hem}, X^*_{usp}, X^*_{mt}), which are calculated as follows:

$$\begin{aligned} X^*_{\text{ilm}} &= \frac{\sqrt{n_{(\text{Ti+Si, F})}\ n_{(\text{Fe}^{2+}\text{, F})}}}{0.5n_{(\text{Fe}^{3+}\text{, F})} + \sqrt{n_{(\text{Ti+Si, F})}\ n_{(\text{Fe}^{2+}\text{, F})}}} \\ X^*_{\text{hem}} &= 1 - X^*_{\text{ilm}} \end{aligned} \tag{6.61}$$

$$\begin{aligned} X^*_{\text{usp}} &= \frac{n_{(\text{Ti+Si, F})}\ X_{(\text{Fe}^{2+}\text{, S}^{2+})}}{0.5n_{(\text{Fe}^{3+}\text{, F})}\ X_{(\text{Fe}^{3+}\text{, S}^{3+})} + n_{(\text{Ti+Si, F})}\ X_{(\text{Fe}^{2+}\text{, S}^{2+})}} \\ X^*_{\text{mt}} &= 1 - X^*_{\text{usp}} \end{aligned} \tag{6.62}$$

where n denotes the number of moles, F is the formula unit, $X_{\text{Fe}^{2+}\text{, S}^{2+}}$ is the mole fraction of Fe^{2+} versus all other 2+ cations, and $X_{\text{Fe}^{3+}\text{, S}^{3+}}$ is the mole fraction of Fe^{3+} versus all other 3+ cations.

Table 6.6 Parameters for the solution model of Spencer and Lindsley (1981).

	Interaction and other parameters*	
	kJ mol^{-1}	**J mol^{-1} K^{-1}**
$A_1 = -3X^2_{usp} + 4X_{usp} - 1$	$W^G_{usp}(T \geq 800°C) = 0$	$W^G_{mt}(T \geq 800°C) = 0$
$A_2 = 3X^2_{usp} - 2X_{usp}$	$W^H_{usp}(T < 800°C) = 64.835$	$W^S_{usp}(T < 800°C) = 60.296$
$A_3 = -3X^2_{ilm} + 4X_{ilm} - 1$	$W^H_{mt}(T < 800°C) = 20.798$	$W^S_{mt}(T < 800°C) = 19.652$
$A_4 = 3X^2_{ilm} - 2X_{ilm}$	$W^H_{ilm} = 102.374$	$W^S_{ilm} = 71.095$
$K_{exch} = (X_{usp}X^2_{hem})/(X_{mt}X_{ilm}{}^2)$	$W^H_{hem} = 36.818$	$W^S_{hem} = 7.7714$
$\Delta H_{exch}{}^0 = 27.799$ kJ mol^{-1}	$\Delta H^0_{usp} = -3.0731$**	$\Delta S^0_{usp} = 10.724$**
$\Delta S_{exch}{}^0 = 4.1920$ J mol^{-1} K^{-1}		

*$W^G = W^H - TW^S$, where W^G, W^H, and are free energy, enthalpy, and entropy exchange parameters, respectively.
**These values represent the intercept and slope of a line on a $G_f^0 - T$ plot, and are not values for 298 K.

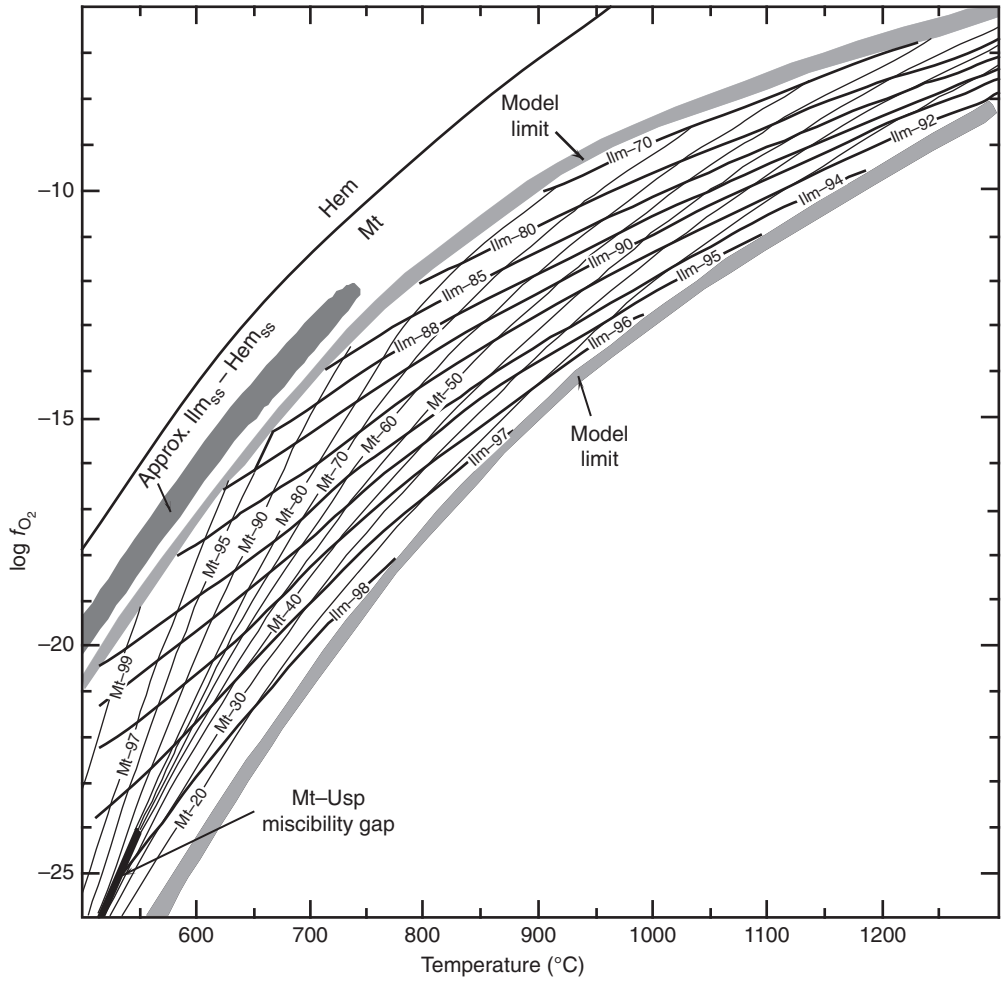

Fig. 6.8 Temperature (°C)– f_{O_2} grid for compositions, in mole percent, of coexisting magnetite (mt)–ulvöspinel (usp) solid solution (mt_{ss}) and ilmenite (ilm)–hematite (hem) solid solution (ilm_{ss}) pairs based on experimental data and the solution model of Spencer and Lindsley (1981). The compositional contours are effectively univariant calibration curves because of the nondetectable effect of pressure on the equilibrium. The intersection of contours for the compositions of these two phases provide a measure of both temperature and oxygen fugacity. The light grey shaded fields are estimates of the limits of the model. The mt–usp miscibility gap is calculated for the three-phase assemblage mt_{ss} + usp_{ss} + ilm_{ss}. The ilmenite–hematite miscibility gap (labeled "Approx. ilm_{ss}-hem_{ss}") is the best guess from experimental data (it is not calculated). The mt_{ss} and ilm_{ss} are assumed to be pure binary Fe–Ti oxides; no minor constituents are considered. (After Spencer and Lindsley 1981, Figure 4, p.1197.)

Example 6–3: Fe–Ti oxide geothermometry and oxygen barometry applied to a sample of Tertiary tholeiitic basalt from Iceland in which the coexisting mt_{ss} and ilm_{ss} have compositions as given in Table 6.7

The results of the first set of necessary calculations are presented in Table 6.8. The first task is to determine $Fe^{2+}$and Fe^{3+} in the mt_{ss} and ilm_{ss} from the total Fe given as FeO. To accomplish this we follow the steps recommended by Stormer (1983): (i) calculate the molar proportions of all cations in the analyses (columns 2 and 3); (ii) normalize the cations in mt_{ss} to a formula unit of 3 sites and the cations in ilm_{ss} to a formula unit of 2 sites (columns 4 and 5); (iii) calculate the sum of the cationic charges per formula unit, and subtract 8 for the mt_{ss} and 6 for the ilm_{ss} (columns 6 and 7) to get the cation charge deficiency (or excess) for each. In the present example, there is a charge deficiency in both cases, which turns out to be 0.3772 for mt_{ss} and 0.1199 for ilm_{ss}.

Table 6.7 Electron microprobe analysis of mtss and ilmss (Carmichael, 1967a).

Wt%	mt_{ss}	ilm_{ss}
SiO_2	0.23	0.17
TiO_2	27.1	49.5
Al_2O_3	1.22	0.13
V_2O_3	0.03	–
Cr_2O_3	0.71	0.10
FeO (t)	67.0	47.8
MnO	0.83	0.49
MgO	0.19	1.09
CaO	0.19	0.16
ZnO	0.12	–
Total	97.6	99.4

FeO (t) = total Fe calculated as FeO.

The charge deficiency numbers show that:

Fe^{3+} cations in the formula unit of mt_{ss} (3 cations total) = 0.3772

Fe^{3+} cations in the formula unit of ilmss. (2 cations total) = 0.1199

To get the number of moles of Fe^{3+} in the formula unit of each solid solution, we subtract the Fe^{3+} cations from its total number of Fe cations:

Fe^{2+} cations in $mt_{ss} = 2.1027 - 0.3772 = 1.7255$

Fe^{2+} cations in $ilm_{ss} = 1.0017 - 0.1199 = 0.8818$

We now have the number of moles of each cation per formula unit for both phases (columns 9 and 10) so that we can calculate the apparent mole fractions of usp in mt_{ss} and of ilm in ilm_{ss}, using equations (6.61) and (6.62).
For mt_{ss}:

$$n_{(\mathrm{Ti+Si,\ F})} = 0.7648 + 0.0086 = 0.7734$$

$$X_{(Fe^{2+},\,S^{2+})} = \frac{n_{(Fe^{2+},\ F)}}{n_{(Fe^{2+},\ F)} + n_{(Mn,\ F)} + n_{(Mg,\ F)} + n_{(Ca,\ F)} + n_{(Zn,\ F)}} = 0.9730$$

$$X_{(Fe^{3+},\,S^{3+})} = \frac{n_{(Fe^{3+},\ F)}}{n_{(Fe^{3+},\ F)} + n_{(Al,\ F)} + n_{(V,\ F)} + n_{(Cr,\ F)}} = 0.8324$$

$$X^*_{usp} = \frac{n_{(\mathrm{Ti+Si,\ F})}\, X_{(Fe^{2+},\,S^{2+})}}{0.5 n_{(Fe^{3+},\ F)}\, X_{(Fe^{3+},\,S^{3+})} + n_{(\mathrm{Ti+Si,\ F})}\, X_{(Fe^{2+},\,S^{2+})}} = 0.8275$$

$$X^*_{mt} = 1 - X^*_{usp} = 0.1725$$

Table 6.8 First set of calculations for Fe–Ti oxide geothermometry and oxygen barometry of Tertiary tholeiitic basalt from Iceland.

	Molar proportion of cations		Normalized to 3 cations for mt_{ss} and 2 cations for ilm_s		Cationic charge			Recomputed molar proportion of cations	
(1)	(2) mt_{ss}	(3)ilm_{ss}	(4)mt_{ss}	(5) ilm_{ss}	(6) mt_{ss}	(7) ilm_{ss}	(8)	(9) mt_{ss}	(10) ilm_{ss}
Si^{4+}	0.0038	0.0028	0.0086	0.0043	0.0345	0.0171	Si^{4+}	0.0086	0.0043
Ti^{4+}	0.3392	0.6195	0.7648	0.9328	3.0591	3.7313	Ti^{4+}	0.7648	0.9329
Al^{3+}	0.0239	0.0025	0.0540	0.0038	0.1619	0.0115	Al^{3+}	0.0540	0.0038
V^{3+}	0.0004	0.0000	0.0009	0.0000	0.0027	0.0000	V^{3+}	0.0009	0.0000
Cr^{3+}	0.0093	0.0013	0.0211	0.0020	0.0632	0.0059	Cr^{3+}	0.0211	0.0020
Fe^{2+} (t)	0.9325	0.6653	2.1027	1.0017	4.2054	2.0035	Fe^{3+}	0.3770	0.1199
Mn^{2+}	0.0117	0.0069	0.0264	0.0104	0.0528	0.0208	Fe^{2+}	1.7256	0.8817
Mg^{2+}	0.0047	0.0270	0.0106	0.0407	0.0213	0.0814	Mn^{2+}	0.0264	0.0104
Ca^{2+}	0.0034	0.0029	0.0076	0.0043	0.0153	0.0086	Mg^{2+}	0.0106	0.0407
Zn^{2+}	0.0015	0.0000	0.0033	0.0000	0.0067	0.0000	Ca^{2+}	0.0076	0.0043
Total	1.3305	1.3283	3.0000	2.0001	7.6228	5.8801	Zn^{2+}	0.0033	0.0000
Cation deficiency					0.3772	0.1199	Total	3.0000	2.0000

Fe^{2+} (t) = total Fe expressed as Fe^{2+}.

For ilm_{ss}:

$$n_{(Ti+Si,\,F)} = 0.9329 + 0.0043 = 0.9372$$

$$X^*_{ilm} = \frac{\sqrt{n_{(Ti+Si,F)}\; n_{(Fe^{2+},\,F)}}}{0.5n_{(Fe^{3+},\,F)} + \sqrt{n_{(Ti+Si,\,F)}\; n_{(Fe^{2+},\,F)}}} = 0.9193$$

$$X^*_{hem} = 1—X^*_{ilm} = 0.0807$$

Next we calculate the following parameters as defined in Table 6.6, replacing X_i values with X_i^* values:

$$A_1 = -3X^2_{usp} + 4X_{usp} - 1 = 0.2557; \qquad A_2 = 3X^2_{usp} - 2X_{usp} = 0.3992$$

$$A_3 = -3X^2_{ilm} + 4X_{ilm} - 1 = 0.1419; \qquad A_4 = 3X^2_{ilm} - 2X_{ilm} = 0.6967$$

$$K_{exch} = (X_{usp}\, X^2_{hem}/X_{mt}\, X^2_{ilm}) = 0.0369$$

Substituting the values calculated above and the low-T parameters (Table 6.6) in equation (6.59), we obtain T = 1622 K (1349°C). Since T is above 800°C, we recalculate T by setting $W^H_{usp} = 0$, $W^S_{usp} = 0$, $W^H_{mt} = 0$, and $W^S_{mt} = 0$, and then use the new value of T to calculate f_{O_2} using equation (6.60), remembering that $W^G_{usp} = 0$ and $W^G_{mt} = 0$ at $T < 800$°C.

The final result: T = 1443 K (1170°C); $\log f_{O_2} = -9.23$.

6.6 Solvus equilibria

As mentioned earlier (section 5.5.1), the unmixing of a non-ideal binary solid solution below the consolute temperature at a given pressure provides a method of geothermometry. For example, the calcite ($CaCO_3$)–dolomite ($CaMg(CO_3)_2$) solvus (Fig. 6.9) can be used to estimate the equilibration temperature from the compositions of calcite coexisting in equilibrium with dolomite. (Strictly speaking, the immiscibility between two phases of different crystal structures, such as calcite and dolomite, is not a "solvus", but for brevity we shall refer to such a miscibility gap as "solvus".). The solvus, however, is not applicable to natural calcites, which generally contain small amounts of $MgCO_3$ and $FeCO_3$ in solid solution.

Reliable experimental data on the ternary $CaCO_3$ – $MgCO_3$ – $FeCO_3$ system are not available. Anovitz and Essene (1987) constructed isothermal phase diagrams for the system from natural carbonate assemblages at various grades of metamorphism and used these to obtain approximate activity–composition relations for the phase components, assuming an asymmetric regular solution model for the ternary system. The equation they derived for the calculation of equilibration temperature from the mole fractions of $CaCO_3$, $MgCO_3$, and $FeCO_3$ in calcite (cal) is:

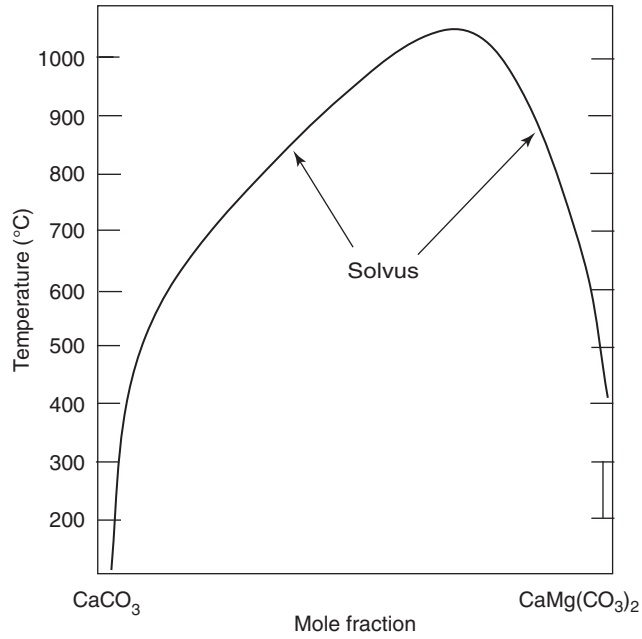

Fig. 6.9 The calcite–dolomite solvus constructed by Anovitz and Essene (1987). The position of the calcite limb of the solvus was based on reversed experiments of several earlier workers. Equilibration temperatures were calculated from the calcite limb of the solvus and natural dolomite compositions in equilibrium with calcites were used to locate the dolomite limb of the solvus. The solvus seems to be well calibrated in the temperature range from 400 to 800°C. (After Anovitz and Essene, 1987, Figure 3, p. 394.)

$$\begin{aligned} T\ (\mathrm{K}) = {} & T_{Fe-Mg} + a(X^{cal}_{FeCO_3}) + b(X^{cal}_{FeCO_3})^2 + c(X^{cal}_{FeCO_3}/X^{cal}_{MgCO_3}) \\ & + d(X^{cal}_{FeCO_3}.X^{cal}_{MgCO_3}) + e(X^{cal}_{FeCO_3}/X^{cal}_{MgCO_3})^2 \\ & + f(X^{cal}_{FeCO_3}.X^{cal}_{MgCO_3})^2 \end{aligned} \tag{6.63}$$

where

$$\begin{aligned} T_{Fe-Mg}(\mathrm{K}) = {} & A(X^{cal}_{MgCO_3}) + B/(X^{cal}_{MgCO_3})^2 + C(X^{cal}_{MgCO_3})^2 \\ & + D(X^{cal}_{MgCO_3})^{0.5} + E \end{aligned} \tag{6.64}$$

and the values of the constants (A, B, C, D, E, a, b, c, d, e, and f) are as given in Table 6.9. Evidently, for very small values of

Table 6.9 Coefficients for equations (6.63) and (6.64) (Anovitz and Essene, 1987).

Coefficient	Value	Coefficient	Value
A	–2360	*a*	1718
B	–0.01345	*b*	–10610
C	2620	*c*	22.49
D	2608	*d*	–26260
E	334	*e*	1.333
		f	0.32837×10^7

$X^{cal}_{FeCO_3}$, the difference in T calculated from equations (6.63) and (6.64) will be very small.

The formulation of Anovitz and Essene (1987) does not consider the possible effect of Mn in calcite, but the mole fraction of Mn in natural calcites is commonly too small to make a significant contribution to the temperature estimate. The two-carbonate thermometer is not recommended for high-temperature metamorphic rocks (above about 600°C) because of possible loss of Mg from the original high-Mg calcite due to exsolution (resulting in dolomite lamellae in calcite) or diffusion during retrogression.

6.7 Uncertainties in thermobarometric estimates

Realistic interpretation of thermobarometric results requires an appreciation of the uncertainties associated with the *P–T* estimates. The calculation of uncertainties is largely an exercise in statistics, which is beyond the scope of the present book. The purpose of this section is to provide an overview of the subject; the details are discussed in many recent publications (e.g., Hodges and McKenna, 1987; Kohn and Spear, 1991; Spear, 1993; Powell and Holland, 1994).

Sources of error in geothermobarometry include (modified from Spear, 1993):

(1) accuracy of calibration, experimental or calculated (in the latter case because of uncertainties of thermodynamic datasets);
(2) error in the ΔV_r;
(3) uncertainty associated with the compositions of standards and matrix correction factors used in electron microprobe analyses;
(4) analytical imprecision in electron microprobe analyses and in the estimation of Fe^{3+} from Fe_{total} such analyses;
(5) cross correlations between errors in temperature estimates (for geobarometers) and errors in pressure (for geothermometers) as all thermobarometers are dependent to some extent on both temperature and pressure;
(6) compositional heterogeneities in minerals; and
(7) uncertainties in activity–composition models for solid solutions.

Items (1) to (5) produce *random errors* that can be handled statistically by standard techniques of error propagation (see, e.g., Hodges and McKenna, 1987; Spear, 1993), whereas items (6) and (7) generate *systematic errors* that are handled differently (see, e.g., Kohn and Spear, 1991; Powell and Holland, 1994). Since the pressure term in the calculations (see, e.g., equation 6.4) is a difference between the pressure of interest and the reference pressure, many of the sources of uncertainty in pressure cancel out. Many of the uncertainties in the *P–T* estimates arise from sources that contribute to error in the temperature estimate, which also contributes to error in the pressure estimate.

Calculated *P–T* estimates are critically dependent on the mixing models adopted for the various solid solution phases involved in the chosen thermobarometric reactions. For example, as shown by Spear (1993, pp. 528–531), the *P–T* obtained for a single set of mineral analyses from Mount Moosilauke, New Hampshire (Sample 90A, Hodges and Spear, 1982), using the calibrations of different authors for garnet–biotite thermometry and GASP barometry, show a spread of approximately 80°C and as much as 3.5 kbar. Without an absolute reference against which the calculated pressures can be compared, it is not possible to make a judgment as to which of these calibrations is the most accurate, and an arithmetic average of the estimates will not be meaningful.

A practical approach for obtaining more consistent *P–T* estimates may lie in using an internally consistent set of thermometers and barometers, which is calibrated either with the same thermodynamic database and solution models for all phases or against the same set of empirical data. The results of such an approach for the same Mt Moosilauke sample 90A mentioned above are shown in Fig. 6.10. The internally consistent thermodynamic data set of Berman (1988) and Holland and Powell (1990) would also yield a consistent set of *P–T* estimates for this sample.

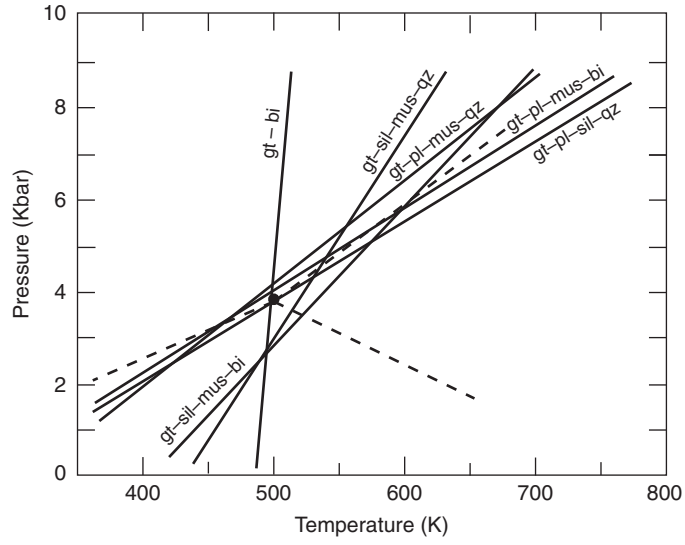

Fig. 6.10 Pressure–temperature diagram showing an internally consistent set of geothermobarometers applied to sample 90A from Mount Moosilauke, New Hampshire. The three garnet–plagioclase geobarometers (gt–pl–mus–qz, gt–pl–mus–bi, gt–pl–sil–qz) give pressures very close to 4 kbar at 500°C, whereas the two plagioclase-absent geobarometers (gt–mus–sil–qz, gt–mus–bi–sil) give slightly lower pressures, with a mean value of approximately 3.25 ± 0.75 kbar. Calibration of the gt–bi geothermometer is from Hodges and Spear (1982) and calibrations of the five geobarometers are from Hodges and Crowley (1985). Phase relations among the Al_2SiO_5 polymorphs are shown for reference. (After Spear, 1993, Figure 15–10, p. 532.)

To obtain optimal results, Powell and Holland (1985, 1994) have proposed a further refinement of the internally consistent approach, which they call "the average *P–T* method". For a given sample (assemblage), this method considers equilibria, including uncertainties and enthalpies of formation of the end-members, pertaining to all possible independent thermobarometric reactions in the system, and employs an iterative least-squares regression technique to calculate an average *P–T* with an ellipse of uncertainty. The calculations are quite complex, but the results can be obtained readily with the computer program THERMOCALC (Powell and Holland, 2001).

It should be pointed out that the internally consistent approach provides a reasonably good test for equilibrium in the assemblage under consideration, but it does not guarantee that the *P–T* estimates are accurate. A consistent set of *P–T* estimates (i.e., with a narrow spread of values) may not be correct because of systematic errors in the calibrations (Spear, 1993).

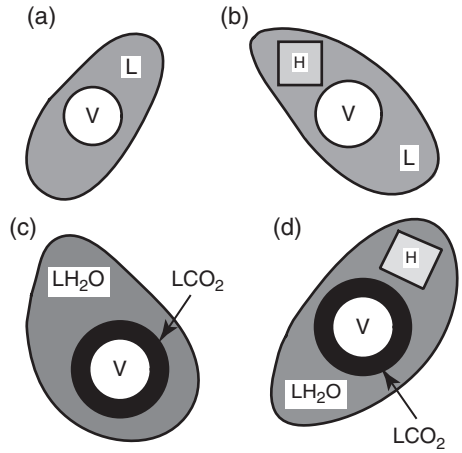

Fig. 6.11 Sketches of some common types of fluid inclusions at room temperature: (a) two-phase (L + V) aqueous inclusion; (b) three-phase (L + V + H) aqueous inclusion; (c) CO_2-bearing inclusion (LCO_2 + V + LH_2O); (d). CO_2-bearing inclusion with a salt crystal (LCO_2 + V + LH_2O + H). Abbreviations: L = liquid, V = vapor, H = halite.

6.8 Fluid inclusion thermobarometry

Fluid inclusions are minute aliquots of fluid that were trapped inside a crystal at some stage of its history. The trapped fluid may be liquid, vapor, or supercritical fluid. In terms of composition, the trapped fluid may be essentially pure water, brines of different salinity (the total dissolved salt content), gas or gas-bearing fluids, or even silicate, carbonate or sulfide melts. Subsequent to trapping at some temperature and pressure, a fluid inclusion may undergo various physical changes (e.g., necking down to form several small inclusions, leakage) and phase transformations (e.g., separation into immiscible gas and liquid phases, crystallization of daughter minerals). At surface temperature–pressure conditions, the inclusions usually consist of some combination of gaseous, liquid, and solid phases (Figs 6.11 and 6.12). The essence of fluid inclusion thermobarometry is to estimate the *trapping temperature* (T_t) and/or *trapping pressure* (P_t) from the present state of the inclusions in a mineral.

This reconstruction requires that the physical characteristics of the fluid inclusions and their behavior during microthermometric analysis (heating and cooling experiments) are consistent with the following assumptions (Roedder, 1984):

(1) the inclusion fluid was trapped and sealed as a single, homogeneous phase;
(2) the inclusion has behaved as an isochoric (constant density) system throughout its history;
(3) nothing has been added to or lost from the inclusion after sealing.

In terms of the timing of trapping of the inclusion relative to the crystallization of the host mineral, fluid inclusions may be classified as *primary*, *secondary*, or *pseudosecondary*. Primary inclusions result from fluids trapped in growth irregularities during the growth of the host crystal. Thus, inclusions trapped along growth surfaces of a crystal are the most obvious examples of primary inclusions. A crystal may be fractured one or more times after its formation and the fractures healed in the presence of fluids; fluids trapped in these fractures result in secondary fluid inclusions, which are most easily identified when they occur along a fracture that crosscuts the entire crystal. A crystal may contain secondary inclusions of several generations, each possibly representing a different fluid. Pseudosecondary inclusions originate from trapping of fluid in a fracture that formed during the growth of the crystal; such inclusions show a distribution similar to that of secondary inclusions but are primary in terms of their age relative to the host crystal, although not necessarily of the same composition as the primary inclusions. Distinction among the three types of fluid inclusions (and different generations of secondary inclusions) in a given sample is of fundamental importance in correlating the fluid inclusion data to geologic processes. The petrographic and morphological criteria listed by Roedder (1984, pp. 43–45) for categorization of fluid inclusions are very useful, but the task can be difficult and sometimes impossible. Nevertheless, for thermobarometry it is imperative that we focus on a *fluid inclusion assemblage* (FIA; Goldstein and Reynolds, 1994) – a group of fluid inclusions that were all trapped at the same time and thus from a fluid of about the same composition at approximately the same temperature and pressure – that represents the fluid event of interest.

The practical and interpretative aspects of fluid inclusion study are quite involved, as discussed by several authors (e.g., Hollister and Crawford, 1981; Roedder, 1984; Shepherd *et al.*, 1985; Bodnar, 2003). The basic principles of thermobarometric application, however, can be illustrated

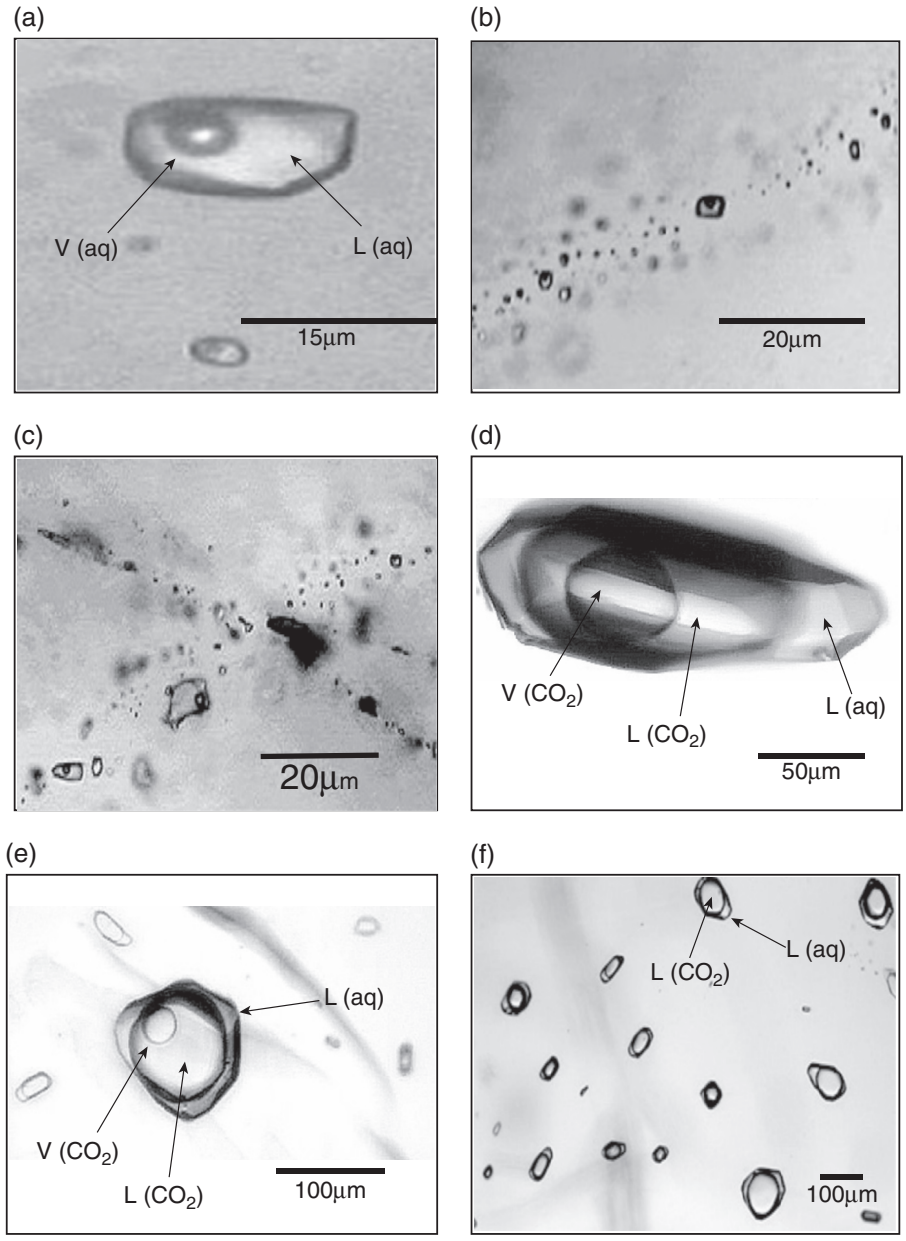

Fig. 6.12 Photomicrographs of fluid inclusions hosted by quartz samples from a gold deposit in India: (a) a two-phase (L + V) aqueous inclusion; (b) secondary aqueous inclusions trapped along a fracture; (c) aqueous inclusions trapped along intersecting fractures; (d) a CO_2–bearing three–phase inclusion; (e) a CO_2–bearing three–phase inclusion; (f) a cluster of CO_2-bearing inclusions. Abbreviations: L = liquid, V = vapor, H = halite. (Courtesy Dr M.K. Panigrahi, Indian Institute of Technology, Khragpur, India.)

by considering an assemblage of two-phase (L + V) aqueous inclusions that can be approximated by the NaCl – H_2O system with no detectable gases, the most common kind of fluid inclusions found in hydrothermal minerals. Suppose we have determined from laboratory experiments that such an assemblage of NaCl – H_2O inclusions have an average salinity (dissolved salt content) of 20 wt% NaCl and an average homogenization temperature (T_h) of 300°C, and that the calculated *P–T* phase relations in this system are as shown in Fig. 6.13. The *homogenization temperature*, the temperature at which an inclusion homogenizes to a single fluid phase, and the vapor pressure in the inclusion at homogenization (P_h; which is about 0.1 kbar in this case) represent T_t and P_t only if the inclusions were trapped in a boiling or immiscible fluid system. In all other cases they represent the minimum values of trapping temperature and trapping pressure,

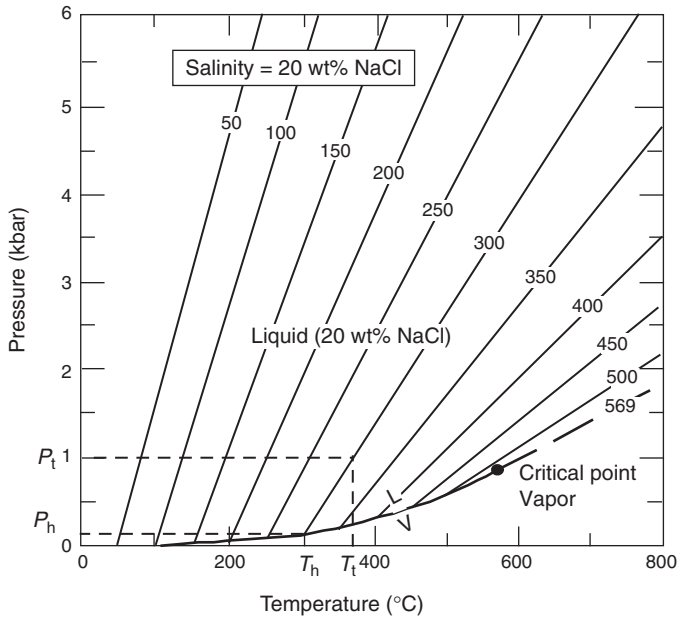

Fig. 6.13 Iso-T_h lines for NaCl-H_2O inclusions having a salinity of 20 wt% NaCl. The L–V curve was constructed using the empirical equations in Atkinson (2002) and the iso-T_h lines using data from Bodnar and Vityk (1994). (After Bodnar, 2003, Fig. 4–10, p. 90.)

irrespective of the fluid composition. Since the fluid inclusions are assumed to have evolved with constant density, the T_t and P_t for this fluid inclusion assemblage are defined by some point along the iso-T_h line (approximately the same as an isochore) marked as 300°C. The liquid (L)–vapor (V) curve in Fig. 6.13 defines the equilibrium between an aqueous solution containing 20 wt% NaCl and a vapor phase of lesser salinity; it was constructed using the empirical equation of Atkinson (2002), which describes the vapor pressure of NaCl – H_2O solutions as a function of salinity and temperature. The iso-T_h lines in this figure were calculated using the equation formulated by Bodnar and Vityk (1994), which calculates the slope of an iso-T_h line as a function of T_h and salinity. As shown in Fig. 6.13 we can use the 300°C iso-T_h line to estimate the T_h as ~370°C if we have an independent estimate of P_t as 1 kbar (e.g., from the thickness of the overlying rocks at the time of trapping or some other geobarometer), and vice versa.

A noteworthy limitation of the approach discussed above is that aqueous inclusion fluids in many geologic environments contain other dissolved salts, such as KCl and $CaCl_2$, in addition to NaCl. At present our ability to use such inclusions for thermobarometry is hindered by (i) the difficulty of observing and identifying phase changes in complex aqueous solutions during heating and cooling experiments (especially in small, natural inclusions) and (ii) the paucity of *P–V–T–X* data applicable to these more complex compositions (Bodnar, 2003).

6.9 Summary

1. Geothermometry and geobarometry refer, respectively, to the estimation of temperature and pressure at which a given mineral assemblage equilibrated during some event in its history (e.g., magmatic crystallization, prograde or retrograde metamorphism, hydrothermal alteration).
2. The tools that have commonly been used for geothermobarometry are: (i) univariant reactions and displaced equilibria; (ii) exchange reactions; (iii) solvus equilibria; (iv) study of cogenetic fluid inclusions in minerals; and (v) fractionation of oxygen and sulfur isotopes between coexisting phases.
3. The dependence of the equilibrium constant of a reaction on temperature and pressure is given by the following equations:

$$\left(\frac{\partial \ln K_{eq}}{\partial T}\right)_P = -\frac{1}{R}\left(\frac{\partial (\Delta G_r^0 / T)}{\partial T}\right)_P$$

$$= \frac{\Delta H_r^0}{RT^2} \quad \text{van't Hoff equation}$$

$$\left(\frac{\partial \ln K_{eq}}{\partial P}\right)_T = -\frac{1}{RT}\left(\frac{\partial \Delta G_r^0}{\partial P}\right)_T = -\frac{\Delta V_r^0}{RT}$$

Since the equilibrium constant is a function of both temperature and pressure, one of the variables must be known from an independent source in order to calculate the other. For a reaction to be a sensitive geothermometer, its equilibrium constant should largely be a function of T, that is the reaction should have a large value of ΔH_r and a small value of ΔV_r; for a reaction to be a sensitive geobarometers, it should have a large value of ΔV_r and a small value of ΔH_r.
4. In general, reactions involving a fluid phase are not suitable for thermobarometry because of a lack of information about the fluid composition and the ratio of fluid pressure (P_f) to total pressure (P_{total}).
5. The basic relation used for calculation of equilibrium temperature and pressure of reactions is

$$\ln K_{eq} = \frac{-\Delta G_r^0}{RT} = \frac{-\Delta H_r^0}{RT} + \frac{\Delta S_r^0}{R}$$

where the superscript "0" refers to the chosen standard state.
6. For univariant reactions and displaced equilibria (net transfer reactions) involving solid phases only,

$$\ln K_{eq} = \frac{-\Delta H_{r,T}^1}{RT} + \frac{\Delta S_{r,T}^1}{R} - \frac{(P-1)\,\Delta V_r}{RT}$$

if the standard state for each substance is taken as the pure substance at the temperature (T) and pressure (P) of interest, and ΔV_r is assumed to be independent of temperature and pressure.

7. For an exchange reaction involving 1 mole each of two elements (or cations) A and B between the phases α and β,

$$K_{eq}(P, T) = K_D\, K_\lambda(P, T)$$

where,

$$K_D = \frac{(X_A/X_B)^\alpha}{(X_A/X_B)^\beta} \text{ and } K_\lambda = \frac{(\lambda_A/\lambda_B)^\alpha}{(\lambda_A/\lambda_B)^\beta}$$

8. Reactions selected for geothermobarometry commonly include one or more solid solutions. The activity–composition relations in such solid solutions depend on the choice of solution models for the particular problem.
9. Rigorous thermobarometry should include an estimate of uncertainties in the estimated temperature and pressure due to several possible sources of error, some of which are random and others systematic.
10. Study of fluid inclusion assemblages can provide reasonable estimates of trapping temperature and trapping pressure if P–V–T–X data are available for the inclusion fluid composition. The application of fluid inclusion thermobarometry to complex compositions is hindered at present by the lack of reliable P–V–T–X data for such systems.

6.10 Recapitulation

Terms and concepts

Al_2SiO_5 triple point
Displaced equilibria
Exchange reaction
Fluid inclusion assemblage
Fluid inclusion microthermometry
Geobarometer
Geobarometry
Geothermometer
Geothermometry
Homogenization temperature
Oxygen fugacity
Petrogenetic grid
Solid solutions
Solvus equilibria
Trapping pressure
Trapping temperature
Univariant reaction
van't Hoff equation

Computation techniques

- Activities of constituents of solid solutions.
- Variation of equilibrium constant as a function of temperature and pressure.
- Reaction boundaries in P–T space.
- Equilibration temperature and pressures of appropriate mineral assemblages.

6.11 Questions

1. Show that for a reaction at constant pressure, the difference in the equilibrium constant at temperatures T_1 and T_2, assuming $(\Delta C_P)_r = 0$, is related to the standard state enthalpy, ΔH_r^0, of the reaction by the relation

$$\ln K_{T_2} - \ln K_{T_1} = -\frac{\Delta H_r^0}{R}\left(\frac{1}{T_2} - \frac{1}{T_1}\right)$$

2. The ΔG^0 (in kJ mol^{-1}) of the reaction

$$\underset{\text{dolomite}}{3CaMg(CO_3)_2} + \underset{\text{quartz}}{4SiO_2} + \underset{\text{fluid}}{H_2O} = \underset{\text{talc}}{Mg_3Si_4O_{10}(OH)_2} + \underset{\text{calcite}}{3CaCO_3} + \underset{\text{fluid}}{3CO_2}$$

can be described by the relation $\Delta G_r^0 = 173.1 - 0.2275T$ at 2 kbar pressure, assuming $(\Delta C_P)_r = 0$ (Powell, 1978, p. 116). How does the equilibrium constant for the reaction change if the temperature of the reaction is raised from 300 K to 700 K? What is the slope of the line in a plot of ln K_{eq} versus $10^3/T$?

3. Calculate the equilibrium metamorphic pressure at 750°C for GAPES and GADS assemblages using the solid solution models discussed in the text. Assume quartz to be a pure phase, no mixing in the octahedral or tetrahedral sites in garnet, and no mixing in the tetrahedral sites in pyroxene. The cation and component mole fractions in the different minerals in the GAPES and GADS assemblages are given below:

Garnet	Plagioclase	Clinopyroxene	Orthopyroxene
$X_{Mg}^{cubic} = 0.181$	$X_{ab} = 0.613$	$X_{Ca}^{M2} = 0.870$	$X_{Mg}^{M2} = 0.482$
$X_{Fe^{2+}}^{cubic} = 0.598$	$X_{an} = 0.373$	$X_{Mg}^{M1} = 0.664$	$X_{Mg}^{M1} = 0.468$
$X_{Ca}^{cubic} = 0.191$			

4. Given below are the compositions of coexisting mt_{ss} and ilm_{ss} in a sample of basalt (Carmichael, 1967b).
Calculate the temperature and oxygen fugacity of equilibration represented by the assemblage. Assume that the

Wt%	mt_{ss}	ilm_{ss}
SiO_2	0.09	0.06
TiO_2	28.80	50.32
Al_2O_3	1.18	0.02
V_2O_3	0.97	0.11
Cr_2O_3	0.71	–
Fe_2O_3	10.74	4.34
FeO	56.06	43.85
MnO	0.82	0.50
MgO	0.50	0.49
CaO	0.14	0.07
ZnO	0.12	–
Total	99.44	99.76

assemblage had achieved equilibrium and has experienced no subsequent change.

5. Given below are the electron microprobe analyses (in wt%) of coexisting garnet and clinopyroxene in an eclogite xenolith recovered from the Udachnaya kimberlite pipe, Siberia (Misra *et al*., 2004):

	Garnet	Clinopyroxene
SiO_2	40.5	55.9
TiO_2	0.55	0.50
Al_2O_3	21.9	11.2
Cr_2O_3	0.06	0.07
MgO	12.2	9.01
FeO (total)	17.3	4.87
CaO	6.95	11.7
MnO	0.34	0.04
Na_2O	0.23	6.67
K_2O	0.04	0.12
Total	100.07	100.08

Calculate the temperature of equilibration using the calibrations of Ellis and Green and (1979) and Krogh (1988), assuming FeO (total) = FeO (i.e., no Fe^{3+} in the garnet or clinopyroxene) and an equilibrium pressure of 6.5 GPa. Comment on the discrepancy, if any, between the two estimates of temperature.

6. The compositions of coexisting garnet and biotite (expressed as mole ratios) in a sample from the sillimanite metamorphic zone in a pelitic schist unit are as follows (Ferry, 1980):

garnet: Fe/(Fe + Mg) = 0.872; and biotite: Fe/(Fe + Mg) = 0.507

Assuming equilibrium at a pressure of 3474 bars, calculate the temperature of metamorphic equilibration of the pelitic schist, using the calibration of Ferry and Spear (1978).

7. Consider the metamorphic assemblage garnet–biotite–plagioclase–kyanite–quartz. Microprobe analyses have shown that in the cubic garnet site $X_{Ca} = 0.04$, $X_{Mg} = 0.18$, and $X_{Fe^{2+}} = 0.78$. The biotite has the octahedral-site contents $X_{Mg} = 0.63$ and $X_{Fe^{2+}} = 0.37$. If the activity of the anorthite component of plagioclase has been calculated to be 0.3, calculate the equilibrium P and T values that are consistent with these mineral compositions. For biotite–garnet equilibrium,

$$\underset{\text{almandine}}{\overset{\text{garnet}}{Fe_3Al_2Si_3O_{12}}} + \underset{\text{phlogopite}}{KMg_3AlSi_3O_{10}(OH)_2} \Leftrightarrow \underset{\text{pyrope}}{\overset{\text{garnet}}{Mg_3Al_2Si_3O_{12}}} + \underset{\text{annite}}{\overset{\text{biotite}}{KFe_3AlSi_3O_{10}(OH)_2}} \quad (6.47)$$

use the following equation calculated from Ferry and Spear (1978):

$$\ln K = \ln\left(\frac{X_{Mg}}{X_{Fe}}\right)_{gt} - \ln\left(\frac{X_{Mg}}{X_{Fe}}\right)_{biot} = -\frac{2089}{T} - \frac{0.0096\,(P-1)}{T} + 0.782$$

For plagioclase–garnet–kyanite–quartz equilibrium,

$$\underset{\text{grossular}}{\overset{\text{gt}}{Ca_3Al_2Si_3O_{12}}} + \underset{\text{kyanite}}{2Al_2SiO_5} + \underset{\text{quartz}}{SiO_2} \Leftrightarrow \underset{\text{anorthite}}{3CaAl_2Si_2O_8}$$

use the following equation calculated from Koziol and Newton (1988):

$$\ln K = \ln\left(\frac{(a_{an}^{plag})^3}{a_{gross}^{gt}}\right) = -\frac{5815}{T} - 0.795\frac{(P-1)}{T} + 18.12$$

In both equations, T is in Kelvin and P is in bars. Calculate the equilibrium temperature and pressure for the mineral assemblage, assuming all the solid solutions to be ideal. (After Nordstrom and Munoz, 1994.)

8. The metamorphic mineral assemblage garnet + plagioclase + orthopyroxene + quartz occurs within granulite facies rocks of pelitic bulk composition. The equilibrium among these minerals can be represented by the reaction

$$\underset{\text{grossular}}{\overset{\text{garnet}}{Ca_3Al_2Si_3O_{12}}} + \underset{\text{almandine}}{\overset{\text{garnet}}{2Fe_3Al_2Si_3O_{12}}} + \underset{}{\overset{\text{quartz}}{3SiO_2}} \Leftrightarrow \underset{\text{anorthite}}{\overset{\text{plagioclase}}{3CaAl_2Si_2O_8}} + \underset{\text{ferosillite}}{\overset{\text{orthopyroxene}}{3Fe_2Si_2O_6}}$$

(a) Calculate the equilibrium constant for the reaction if the composition of the minerals at equilibrium are as follows:

garnet: $Ca_{1.04}Fe_{1.43}Mg_{0.46}Mn_{0.07}Al_{2.15}Si_{2.86}O_{12}$
plagioclase: $Ca_{0.91}Na_{0.07}K_{0.02}Al_{2.35}Si_{1.65}O_8$
orthopyroxene: $Ca_{0.09}Fe_{1.67}Mg_{0.19}Al_{0.07}Si_{1.98}O_6$

Assume that the solid solutions are ideal (i.e., $a = X^n$, where X = mole fraction and n = site multiplicity).

(b) From the P–T calibration of this reaction by Bohlen *et al.* (1983a) estimate the equilibrium pressure corresponding to a temperature of 850°C.

9. In Koziol and Newton (1988), as cited in the question 7, the experimental fit to the univariant line for the reaction

$$\underset{\text{grossular}}{Ca_3Al_2Si_3O_{12}} + \underset{\text{kyanite}}{2Al_2SiO_5} + \underset{\text{quartz}}{SiO_2} \Leftrightarrow \underset{\text{anorthite}}{3CaAl_2Si_2O_8}$$

is given by

P (bars) = 22.80 T (°C) – 1093

Derive the ln K equation used in the above problem from the P–T fit to the experimental data. Take $\Delta V_{(s)} = 6.608$ J bar^{-1}. Note that the temperature scales are different. State any assumptions that you need to make. (After Nordstrom and Munoz, 1994.)